Polymer-Based Technologies for Sensing Applications

Wildemar S. P. Carvalho, Menglian Wei, Nduka Ikpo, Yongfeng Gao, Michael J. Serpe*
Department of Chemistry, University of Alberta, Edmonton, AB, T6G 2G2 Phone: (780) 492-5778
Email: serpe@ualberta.ca

1. Introduction

Reports in the literature on the development of new chemical sensing technologies have been growing steadily in number for years. For example, a Web of Science topic search using the term "Chemical Sensing" revealed that over 8,000 papers were published in 2015-2017, with over 40,000 citations to those papers. In this review, we focus on highlighting recent examples of chemical sensing related to human health (e.g., disease diagnosis, health monitoring, and water/food safety), and for environmental monitoring. These respective fields were chosen to due to their immense importance. For example, Alzheimer's disease is a chronic progressive neurodegenerative disorder that causes loss of memory (short-term memory loss) and with time, problems associated with cognitive ability and language. Although there is no cure for the disease, early diagnosis is key to access therapies that can improve a patient's cognition and enhance their life quality.[1] Moreover, the development of biosensors for biomarkers of Alzheimer's disease can also be used to track the development of the disease and the impact of treatment. Another important application of chemical sensors is for determining the safety of drinking water supplies. For example, bacterial infectious agents such as *Escherichia coli* (*E. coli*) can cause many health related problems such as diarrhea, abdominal pain, fever, and in more severe cases can lead to death.[2] Finally, chemical sensors can be used to detect contaminants in water bodies that can impact the health of the environment. For example, industrial effluents can lead to unnaturally high concentrations of nutrients in water bodies that

can lead to algae blooms that starve water of oxygen and ultimately kill marine life within that zone. Therefore, technologies that can detect high levels of nutrients (or any of a number of contaminants) in water can allow for the source of the release to be pinpointed and the problem remedied before extensive environmental damage can be done.

Traditional analytical detection methods used for the above mentioned applications generally involve sophisticated instrumentation,[3] highly trained personnel and detailed protocols[4] that prevents their ready use by members of the public and/or those in resource limited areas. Therefore, developing sensing technologies that are inexpensive and easy to use, combined with being sensitive enough to detect relevant concentrations of species of interest (analytes) is of great importance. While there have been many advances in achieving sensors with the desired properties listed above, more progress is needed to develop sensors that are increasingly sensitive, inexpensive, selective, and easy to use in resource limited settings where these technologies need to be incredibly robust and not dependent on access to electricity, running water, and/or climate control.[5] To generate sensors and biosensors with enhanced performance, many have turned to polymer-based technologies. These polymeric materials include hydrogels, molecular imprinted polymers (MIP), conducting polymers and their composites, which have been utilized to fabricate highly responsive sensors and biosensors.[6-8] Often, the polymer-based materials used in these technologies serve to enhance target molecule capture, act as a matrix for functional molecule immobilization (e.g., fluorophores,[9] metal nanoparticles,[10-11] and quantum dots[12-14]), and/or transfer the target capture into a detectable signal by changing its physical/chemical characteristics.[15-18] Other advantages of polymer-based materials are that their chemistry can be easily modified to tune their reactivity, flexibility/stretchability, biocompatibility, and resistance to degradation.

This review highlights select uses of polymers in chemical sensing technologies since 2015. We focus on examples that showcase their use for human health and environmental applications. In each of the examples, we focus on the detailing the polymer's use to achieve the desired application, and the figures of merit (limit of detection (LOD), limit of quantification (LOQ), selectivity, and stability) for the described sensing platforms.

2. Polymer-Based Biosensors for Health Care Monitoring

Over the last few decades, the quality of life has been dramatically improved by the unprecedented growth in technology development. Most of the increase in life expectancy has been driven by several factors, such as food security, large-scale production of essential drugs and the development of novel medical technologies and procedures. The rapid diagnosis of disease by monitoring the concentration of various biochemical compounds (biomarkers) in the body is essential for the timely commencement of relevant, and in some cases lifesaving, therapies. Furthermore, by monitoring the concentration of these biomarkers over time, one can characterize the stage of disease and evaluate the efficacy of therapy. For example, quantifying the amount of cholesterol in blood is important for diagnosing coronary heart disease, arteriosclerosis, and cerebral thrombosis. Real-time, reliable, and accurate diagnostic tools that are capable of monitoring a patient's health wherever the patient is located are highly desirable. The unique properties of polymers have been exploited for such diagnostic tool development, which can be used for the analysis of clinically pertinent biomarkers including proteins, nucleotides, and metabolites. Some reviews have already been published focusing on the development of polymer-based sensors for health monitoring systems.[19-22] Herein, we will

mainly highlight the use of polymer-based materials in sensing technologies for biomedical applications.

2.1 Protein Biosensors

Protein biomarkers (and cytokines in particular) play an essential role for early diagnosis of disease, assessing the stage of the disease, and monitoring the response of the disease to therapy. Cytokines, chemokines, growth factors, and other proteins in physiological fluids and tissues can serve as potentially useful biomarkers.[23-24] For example, tumor necrosis factor-α (TNF-α), a pro-inflammatory cytokine, is a 157-amino acid long polypeptide found at very low concentrations in various physiological fluids such as saliva, plasma, and serum.[25] It mediates a variety of cell functions, including the triggering of nitric oxide (NO) production, which has been associated with a wide range of immune and inflammatory processes such as rheumatoid arthritis[26], neurodegenerative diseases (e.g., Alzheimer's and Parkinson's disease),[27] diabetes, stroke, HIV infection, heart disease, leukemia, and epithelial ovarian cancer.[25, 28-29] Conventional technologies commonly used to measure the concentration of a specific protein in samples involves the use of cell culture, chromatography/mass spectrometry (MS), or enzyme-linked immunosorbent assay (ELISA). However, these techniques can be tedious, time consuming, and rely heavily on expensive and sophisticated instruments, and well-trained personnel.[5, 30] Hence, developing sensors that can detect low levels of protein biomarkers in physiologically relevant samples is crucial for clinical diagnostics. To achieve such a sensor, Sharma *et al.* reported a label-free electrochemical impedance biosensor for the detection of human interleukin-8 (IL-8) in serum.[31] They utilized a gold electrode coated with a self-assembled monolayer (SAM) of monothiol-alkane-poly(ethylene glycol)-acid ($HS\text{-}C_{11}\text{-}(EG)_6\text{-}OCH_2\text{-}COOH$) that was

subsequently modified with a synthetic non-antibody capture protein that had a high affinity for IL-8 via 1-ethyl-3-(3-dimethylaminopropyl)carbodiimide/N-hydroxysuccinimide (EDC/NHS) coupling chemistry. In this case, the protein-modified SAM was able to bind to human IL-8 that changed the sensor's impedance in a manner that depends on IL-8 serum concentration. The sensor was highly immune to non-specific adsorption of proteins from serum due to the presence of the poly(ethylene glycol) units, making the sensor specific for IL-8. The sensor showed a linear response for IL-8 from 9 fg mL^{-1} to 900 ng mL^{-1} and a detection limit of 90 fg mL^{-1}.

Conjugated/conducting polymers have been used extensively in sensing systems due to their easy processability, flexibility and metal-like electronic conductivity. The conductivity of conjugated polymers is a result of contiguous sp^2 hybridization of the carbon backbone in the polymer. For example, Aydin *et al*. recently reported a highly sensitive electrochemical sensor based on indium tin oxide (ITO)-modified flexible polyethylene terephthalate substrates (PET) for TNF-α detection in human serum.[32] They used the conjugated polymer poly(3-thiophene acetic acid) (P3) as an immobilization matrix to increase the surface area of the immunosensor and increase the number of active sites for TNF-α binding. The ITO surface was hydroxylated followed by covalent attachment of the P3 conjugated polymer and subsequent covalent immobilization of the anti-TNF-α antibody onto the P3 polymer using EDC/NHS chemistry. The binding of the surface-bound anti-TNF-α antibody to the TNF-α antigen from human serum, leads to an increase in the semicircle diameter of the electrochemical impedance spectra (EIS) due to obstruction of electron transfer to the electrode surface. Thus, the EIS response corresponded to the increased concentration of TNF-α, which showed a broad linear response for TNF-α from 0.01 to 2 pg mL^{-1}, LOD of 3.7 fg mL^{-1} with high sensitivity, selectivity and good reproducibility.

In another example, Yáñez-Sedeño's group reported the fabrication of an electrochemical platform for the simultaneous determination of two important cytokines: interleukin-1 beta (IL-1β) and TNF-α.[33] IL-1β is a pro-inflammatory cytokine produced by a variety of cells including pancreatic cells, adipocytes or macrophages, while TNF-α plays a critical role in many diseases including rheumatoid arthritis and cancer. They employed dual screen-printed carbon electrodes (SPCEs) modified with 4-carboxyphenyl-functionalized double-walled carbon nanotubes (HOOC-Phe-DWCNTs) as electrochemical scaffolds for immobilization of the specific antibodies. The capture antibodies were immobilized onto HOOC-Phe-DWCNTs/SPCEs using the commercial polymeric coating Mix&Go™, which contains several metallic complexes with a high efficiency to bind proteins. To detect the cytokine targets (IL-1β and/or TNF-α), the modified electrodes were exposed to their respective solutions followed by addition of a biotinylated antibody solution (biotin-anti-IL or biotin-anti-TNF), which can bind the surface-bound target. Finally, poly-horseradish peroxidase (HRP)-streptavidin conjugates were added to the electrode surface that bind the biotinylated antibodies and exposed to the redox mediator hydroquinone and then H_2O_2. Upon application of a detection potential of 0.20 V, a steady state current could be achieved that corresponded to the reduction of benzoquinone, and ultimately the concentration the respective antigens. Under optimum conditions, the biosensor exhibited linear ranges of 0.5 to 100 pg mL^{-1} and from 1 to 200 pg mL^{-1} for IL-1β and TNF-α, respectively and limits of detection were 0.38 pg mL^{-1} (IL-1β) and 0.85 pg mL^{-1} (TNF-α).

In a bid to improve the sensitivity of biosensors, a variety of nanocomposites have been considered.[34-37] For example, recent work by Yang *et al*.[38] described the fabrication of a novel label-free electrochemical biosensor for the detection of carcinoembryonic antigen (CEA), which is one of the most widely used tumor biomarkers for colorectal cancer and other select

carcinomas.[39] The sensor uses a three-dimensional (3D) gold nanoparticle (AuNP)/prussian blue-poly(3,4-ethylenedioxythiophene) (PB-PEDOT) nanocomposite immobilized on a glassy carbon electrode (GCE) as shown in Figure 1a. The AuNPs were loaded on the PB-PEDOT nanocomposites by a simple electrochemical deposition followed by immobilization of the CEA antibody to give (AuNPs/PB-PEDOT)-Anti-CEA. The (AuNPs/PB-PEDOT)-Anti-CEA binds specifically to CEA yielding a current change in the differential pulse voltammograms that depends on the solution concentration of CEA as shown in Figure 1b. After the immunosensor was exposed to various concentrations of CEA, it was noted that the peak current decreased gradually with increasing concentration of CEA. This decrease in peak current was attributed to the insulating effect of the antigen-antibody complex. The developed sensors showed a dynamic range 0.05-40 ng mL^{-1} and detection limit of 0.01 ng mL^{-1} for CEA in human serum samples in Figure 1c.

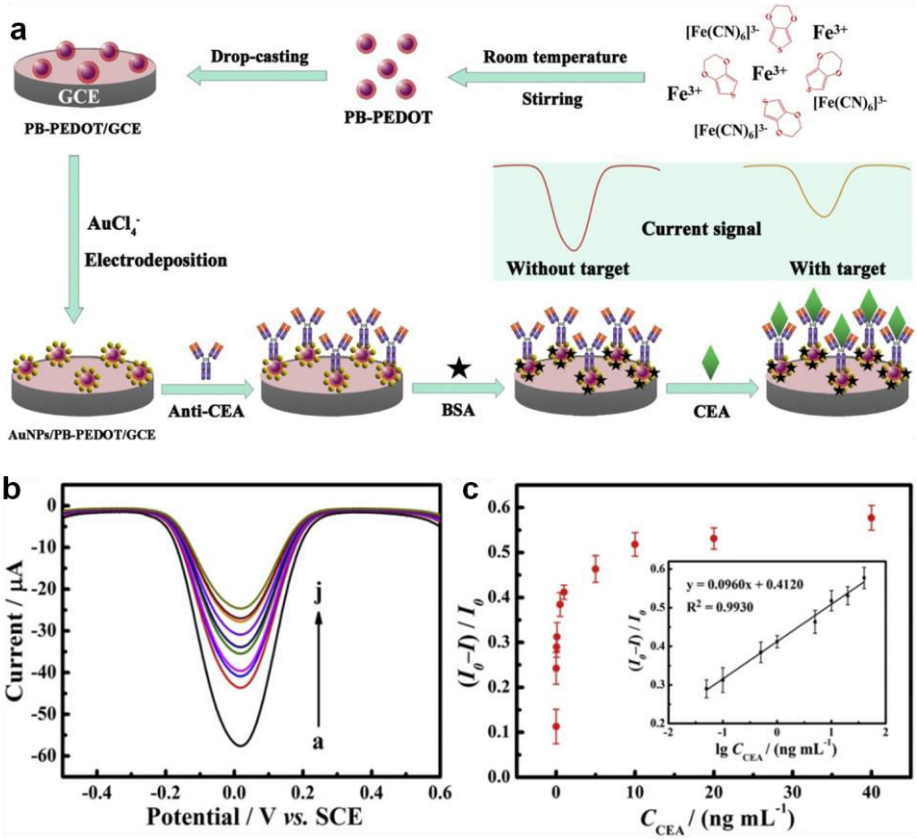

Figure 1. a) The fabrication process of the immunosensor. b) Differential pulse voltammetry of the immunosensor after being incubated with different concentrations of CEA (a–j: 0, 0.01, 0.05, 0.1, 0.5, 1, 5, 10, 20 and 40 ng mL^{-1}). c) Calibration curve for CEA determination. (Inset) Linear plot of the immunosensor inhibition ratio *vs* logarithmic concentration of CEA.[38] Adapted from Sensors and Actuators B: Chemical, Vol. 239, Yang, T.; Gao, Y.; Liu, Z.; Xu, J.; Lu, L.; Yu, Y. Three-dimensional gold nanoparticles/prussian blue-poly(3,4-ethylenedioxythiophene) nanocomposite as novel redox matrix for label-free electrochemical immunoassay of carcinoembryonic antigen, pp. 76-84 (ref 38). Copyright 2017, with permission from Elsevier.

Polymer-based hydrogels are hydrophilic macromolecular networks that are able to absorb and retain large amounts of water. Hydrogels have attracted widespread attention for use in biosensor technologies due to their high water content similar to natural tissue, tunable

chemistry, good biocompatibility, effective anti-fouling properties, elasticity, and toughness.[40] In one example, a conductive hydrogel was prepared utilizing the interactions between 1,3,5-benzenetricarboxylic acid and Fe^{3+} and used as a sensitive label-free electrochemical immunosensor.[41] The hydrogel film was formed on a GCE via a drop coating method followed by electrodeposition of AuNPs on the hydrogel film and subsequent immobilization of the neuron-specific enolase (NSE) antibody onto the AuNPs. The specific binding of NSE, a lung cancer biomarker, was determined using square wave voltammetry (SWV), in which the current response of the immunosensor was shown to decrease with an increase in NSE concentration. The current decrease was attributed to the increased insulating properties as NSE proteins were adsorbed onto the electrode, which retarded electron transfer. The developed immunosensor exhibited a wide linear range of 1 pg mL^{-1} to 20 ng mL^{-1} and LOD of 0.26 pg mL^{-1}.

Molecularly imprinted polymers (MIPs) have been used for the development of sensors and biosensors due to their improved ability to selectively bind molecules of interest compared to non-imprinted polymers.[42-44] MIPs are generated by performing polymerization and crosslinking reactions in the presence of a molecule of interest (analyte). Once the analyte is removed from the resultant polymer-based material, a cavity is left behind that is templated (both the cavity shape and functional group orientation) to bind the analyte once again. The interaction between the polymer network composed of functional monomers and the template molecule normally involves H-bonding and/or other weak intermolecular interactions like π-π interactions, and Van der Waals forces. In addition, MIPs retain the other advantages that polymers have over other non-polymer-based materials. In one example, Liu and co-workers described water-dispersible molecularly imprinted conductive polyaniline (MIP-PANI) particles, which they utilized in the fabrication of an electrochemical sensor for the selective detection for ovalbumin (OVA).[45] The

MIP-PANI, which functions as the molecular recognition element, was prepared by first synthesizing the amphiphilic copolymer poly(2-acrylamido-2-methyl-1-propanesulfonic acid) (AMPS) and polystyrene (St) p(AMPS-co-St), which coassembles with PANI in aqueous solution to generate PANI particles via electrostatic interactions. OVA was used as a template protein, which was added and trapped in the PANI nanoparticles during this process resulting in the formation of MIP-PANI particles. In this investigation, the authors used differential pulse voltammetry (DPV) to monitor the peak current generated by the $[Fe(CN)_6]^{3-/4-}$ probe migrating through the MIP-PANI film and to the electrode surface, which is hindered/blocked when OVA binds to the imprinted sites in the film. As a result, when more OVA was in solution, there was more bound in the film, which led to a concomitant decrease in peak current in the voltammograms. The imprinted PANI sensor exhibited good selectivity toward target protein with a wide linear range for OVA from 10^{-11} to 10^{-6} mg mL^{-1} and a lower detection limit of 10^{-12} mg mL^{-1}.

In another investigation, a sensor for the cardiac biomarker myoglobin (Myo) was fabricated using a combination of MIP and screen-printed electrodes (SPE).[46] The molecular receptor of the sensor was prepared through electrooxidative polymerization of phenol on gold SPE (AuSPE) using Myo as the template molecule. In this investigation, the analytical response of the biosensor was optimized by varying the thickness of the polyphenol nanocoating. It was found that the optimum thickness was ~4.4 nm, which is similar to the protein diameter. The modified surfaces were coated with a 45 μL drop of 5 mM ferro/ferricyanide ($[Fe(CN)_6]^{3-/4-}$), which was the redox probe. SWV was used to monitor the ferro/ferricyanide probe response upon Myo binding on the MIP receptor surface. The peak current obtained by SWV was plotted as a function of the logarithm of Myo concentration (in ng mL^{-1}), affording a wide linear range

from 0.01 ng mL^{-1} to 100 g mL^{-1} in diluted artificial serum and 0.001 ng mL^{-1} to 100 g mL^{-1} in phosphate-buffered saline (PBS). LODs of 2.1 pg mL^{-1} and 14 pg mL^{-1} were obtained in PBS and artificial serum, respectively, indicating that the resulting sensor was capable of detecting Myo at clinically relevant levels.

Shen *et al.*[47] reported an ultra-sensitive human chorionic gonadotropin (hCG) sensor based on surface imprinting by taking advantage of covalent binding and electropolymerization. Specifically, a GCE was modified with multi-walled carbon nanotubes (MWCNTs) and chitosan via layer-by-layer assembly. The electrode was modified with hCG and subsequently electropolymerized with dopamine, which formed a thin, hydrophilic and biocompatible polydopamine (PDA) film. As a result of the lack of conductivity of hCG, electrochemical detection was performed in potassium hexacyanoferrate III ($K_3[Fe(CN)_6]$) and potassium hexacyanoferrate II ($K_4[Fe(CN)_6]$) trihydrate solution that acted as a redox probe. DPV was used to monitor the electrochemical responses of the probe upon binding of the target protein. The response of the electrode to $[Fe(CN)_6]^{3-/4-}$ clearly decreased after it was incubated with hCG. This suggested that hCG binding blocked the pervasion of the hexacyanoferrate probes to the surface thus preventing the redox reaction. It was shown that the peak current decreased gradually with the increase of hCG concentration. The imprinted sensor exhibited high sensitivity with a wide linear range from 0.5 pg mL^{-1} to 250 ng mL^{-1} and a detection limit of 0.035 pg mL^{-1}.

In an effort to exploit fluorescence quenching for sensing applications, a novel turn-on fluorescence sensing strategy for proteins based on supramolecular dissociation was developed by Thayumanavan and coworkers.[48] The detection strategy relied on the fluorescence emission

of a hydrophobic fluorophore covalently attached to a protein-specific ligand (probe). Unlike most sensing strategies using fluorophores where the decrease in florescence intensity is related to the presence/concentration of the target analyte, this example showed an increase in fluorescence intensity in the presence of a target. In this system, the probe was buried in the core of a micelle along with a hydrophobic fluorescence quencher. The authors chose the particular poly(ethylene glycol)-based micelles due to their ability to exchange their inner solution with the bulk. Hence, when the analyte (in this case human carbonic anhydrase I (HCA)) was exposed to the micelles, they bound the probe in the micelle, which allowed some of the analyte-bound probe to diffuse out of the micelle core and away form the quencher. This caused the fluorescence emission intensity of the probe to increase in a manner that depended on the analyte concentration. The authors reported that this simple turn-on fluorescence strategy could selectively detect the presence of HCA at a concentration of 50 nM.

2.2 Nucleic Acid Biosensors

Detection of specific DNA sequences is crucial for early clinical diagnosis of disease and prediction of a diversity of human genetic diseases and pathogenic infections.[49] In recent years, electrochemical biosensors for DNA have been receiving increased attention for the detection of clinical biomarkers due to their simplicity, portability, high sensitivity and selectivity, fast response as well as low fabrication cost and ease of miniaturization that is ideal for point-of-care (POC) applications.[15, 50] Several reviews have described different approaches for optimizing the analysis of DNA using biosensors.[39, 51-53] Although great advances have been reported, the sensitivity and reproducibility of electrochemical biosensors has remained a challenge.[54] Nonetheless, significant work has been reported in the literature on the utilization of smart

materials to circumvent the aforementioned limitations of DNA sensors. In the biosensing field, electrocatalytic materials such as conducting polymers and their composites have been playing an essential role as platforms for biosensor electrode modification especially where increases in the electronic conductivity is required.[55] In one example, Miodek *et al*.[56] synthesized a composite material using a polypyrrole (PPy) film and poly(amidoamine) fourth generation dendrimers (PAMAM G4), in which the PPy layer was first generated using electrochemical polymerization of pyrrole on a gold electrode. The PPy film was then modified with PAMAM G4 via amine electro-oxidation. Subsequently, ferrocenyl groups (Fc) modified with two phthalimidyls were attached to the surface as a redox marker via formation of a peptide bond with PAMAM G4, resulting in the modified nanomaterial (PPy-PAMAM-Fc). Then a ssDNA probe modified with an amine group on the 5' position was anchored to the unreacted phthalimidyl on ferrocene as shown in Figure 2. The obtained ssDNA-modified PPy-PAMAM-Fc nanomaterial was evaluated as a platform for DNA sensing by directly monitoring the redox signal of ferrocene using SWV, which exhibited a decrease in the observed current from ferrocene after incubation with the ssDNA target (DNA_C). The authors attributed the observed phenomenon to the slowed electron transfer efficiency of the ferrocenyl groups or to the slow diffusion of electrolyte to the surface after binding DNA_C. The authors showed that the decrease in the observed current was proportional to the amount of hybridized DNA_C. The sensors showed a broad dynamic range with two linear ranges, from 10 fM to10 pM and from 100 pM to 100 nM with LOD of 0.4 fM.

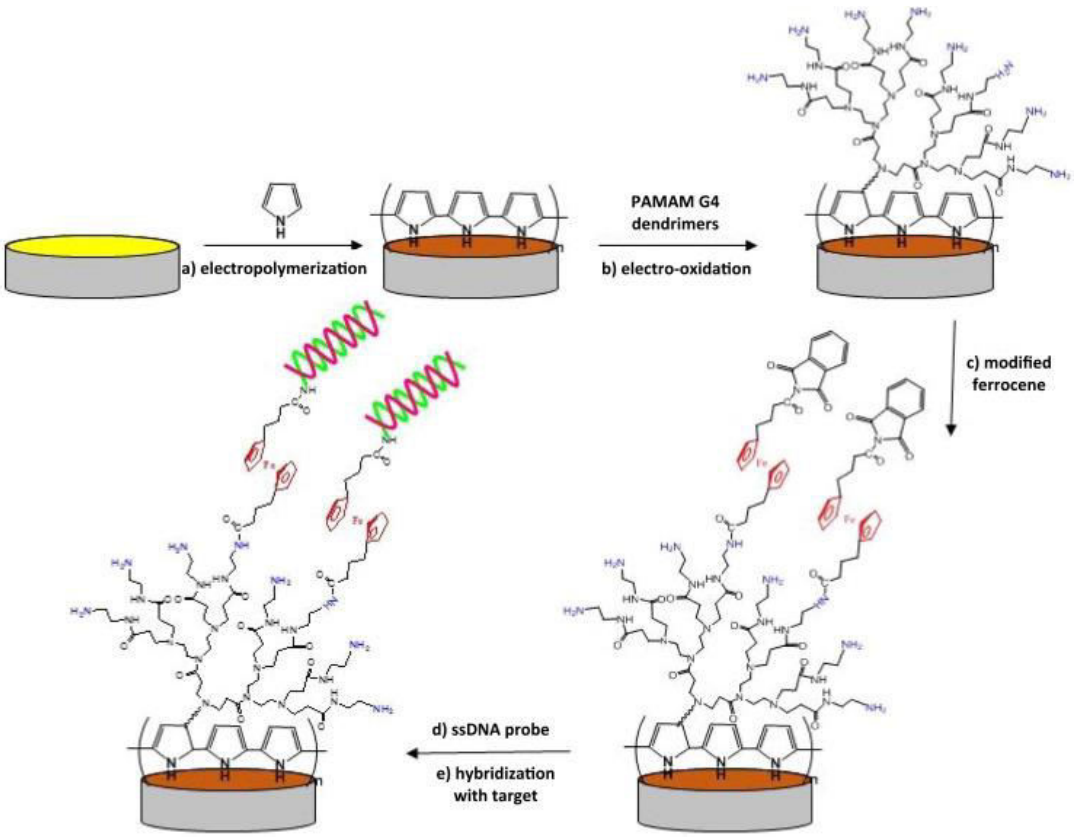

Figure 2. A schematic depiction of a DNA sensor based on modified PPy: (a) electropolymerization of PPy film; (b) electrodeposition of PAMAM G4; (c) covalent grafting of ferrocene; (d) anchoring of ssDNA probe; (e) detection of specific target.[56] Reprinted from Talanta, Vol. 154, Miodek, A.; Mejri-Omrani, N.; Khoder, R.; Korri-Youssoufi, H. Electrochemical functionalization of polypyrrole through amine oxidation of poly(amidoamine) dendrimers: Application to DNA biosensor, pp. 446-454 (ref 56). Copyright 2016, with permission from Elsevier.

Another novel electrochemical DNA biosensor was developed by Zhu *et al*. that utilized PANI-capped bismuth sulfide (rBi_2S_3) nanorods (PANI-rBi_2S_3).[57] The strategy involved depositing rBi_2S_3 particles on ionic liquid-carbon paste electrode (IL-CPE) consisting of 1-butyl-3-methylimidazolium hexafluorophosphate (BMIMPF6) and graphite powder. Subsequently, the

PANI-rBi_2S_3 nanocomposite was generated by electrodeposition of the PANI polymers on the rBi_2S_3 surface. Finally, the probe DNA was attached on the nanocomposite via electrostatic interactions. The authors used nanorod composites to increase the surface area for DNA capture and enhance the conductivity. Upon hybridization of the probe-target DNA, the conductivity changed on the surface of the electrode that was monitored via electrochemical impedance. The dynamic detection range was determined to be from 1.0×10^{-15} to 1.0×10^{-11} M with a detection limit of 4.37×10^{-16} M.

In another investigation, a similar electrochemical biosensor was reported that used PANI and graphene oxide (GO) nanosheet nanocomposites modified on a GCE (PANI/GO/GCE) for DNA detection.[58] The electrode was kept in NHS/EDC solution for activation of the carboxylic acid groups of GO before the immobilization of the probe ssDNA on the electrode surface to obtain the ssDNA/PANI/GO/GCE electrode. Determination of complementary DNA strands in the genomic samples (extracted from human blood) was performed by EIS. DNA hybridization or formation of a complex can cause changes in the conductivity of the recognition layer, therefore by analysis of the semicircle in the Nyquist plots, the charge transfer resistance could be determined. By immersing the prepared electrode surface containing the probe DNA in solutions spiked with different concentrations of target DNA, the authors showed that the charge transfer resistance values increased with increasing concentrations of complementary target DNA. The sensor yielded a linear dynamic range of DNA detection of 1.0×10^{-16} M to 1.0×10^{-8} M and a detection limit of 3.3×10^{-17} M.

Gong *et al.*[59] described a sensitive impedimetric DNA biosensor for HIV-1 gene detection. The biosensor was composed of a GCE modified with a graphene-Nafion composite,

which was used as the sensing platform to immobilize the capture probe ssDNA via π–π stacking interactions. The Nafion was used to both stabilize the graphene and increase its dispersion, which could lead to better sensor performance. The performance of the DNA biosensor was assessed by measuring the dependence of electron transfer resistance on the concentration of the HIV-1 gene using EIS. In the measurement of the HIV gene, the target ssDNA bound to the probe ssDNA, forming double-stranded helix DNA (dsDNA). The formation of the helix allowed its release from the surface of the biosensor, which finally led to an observed electron transfer resistance decrease. The decrease in the electron transfer resistance could be related to the concentration of HIV-1 gene over the range of 1.0×10^{-13} to 1.0×10^{-10} M, with LOD of 2.3×10^{-14} M.

2.3 Metabolite Sensors

The sensing of intermediates and byproducts of metabolism in blood, such as glucose, cholesterol, hydrogen peroxide, urea, lactate and creatinine, is essential in human disease diagnosis and health care monitoring as they are indicators of various diseases.[60] For instance, lactate can be produced through a glycolytic pathway and its concentration is associated with various biological processes including tumor cell metastasis and head trauma. Therefore, the detection and quantification of metabolites is of great importance.[61] In this section, we review recent progress in the development of polymer-based metabolic biosensors.

2.3.1 Glucose

The level of glucose in human blood is closely related to diabetes mellitus, which is one of the leading causes of morbidity and mortality worldwide.[62] Therefore, diabetic patients are

required to regularly measure and track their blood glucose concentration, which makes the development of low cost glucose biosensors capable of the rapid and accurate quantitation of blood glucose concentrations very important.

Typically, enzymatic glucose biosensors exploit the oxidation of glucose into gluconolactone facilitated by the glucose oxidase (GOx) as an enzyme.[63] Recent efforts have focused on enzyme modification for improved sensor performance. Specifically, various polymers and their composites have been explored to enhance electron transfer between the enzyme and electrodes. For example, Kumar-Krishnan *et al.* reported an enzymatic glucose electrochemical biosensor utilizing a GCE that was modified with chitosan supported silver nanowires (CS-AgNWs) and GOx as shown in Figure 3a.[64] The use of the CS-AgNWs platform enabled the self-assembly of the GOx adjacent to the GCE surface, thereby enhancing the direct electron transfer from the electrode to GOx for its redox reaction. By monitoring the current change in the cyclic voltammogram upon glucose addition, a calibration curve can be obtained with a linear range of 1–15 mM and a sensitivity of 16.72 mA mM^{-1} cm^{-2} as shown in Figure 3b. In addition, this electrochemical biosensor showed good resistance to interference from the presence of other species such as acetic acid, citric acid, lactic acid, and uric acid with negligible signal response observed in Figure 3c.

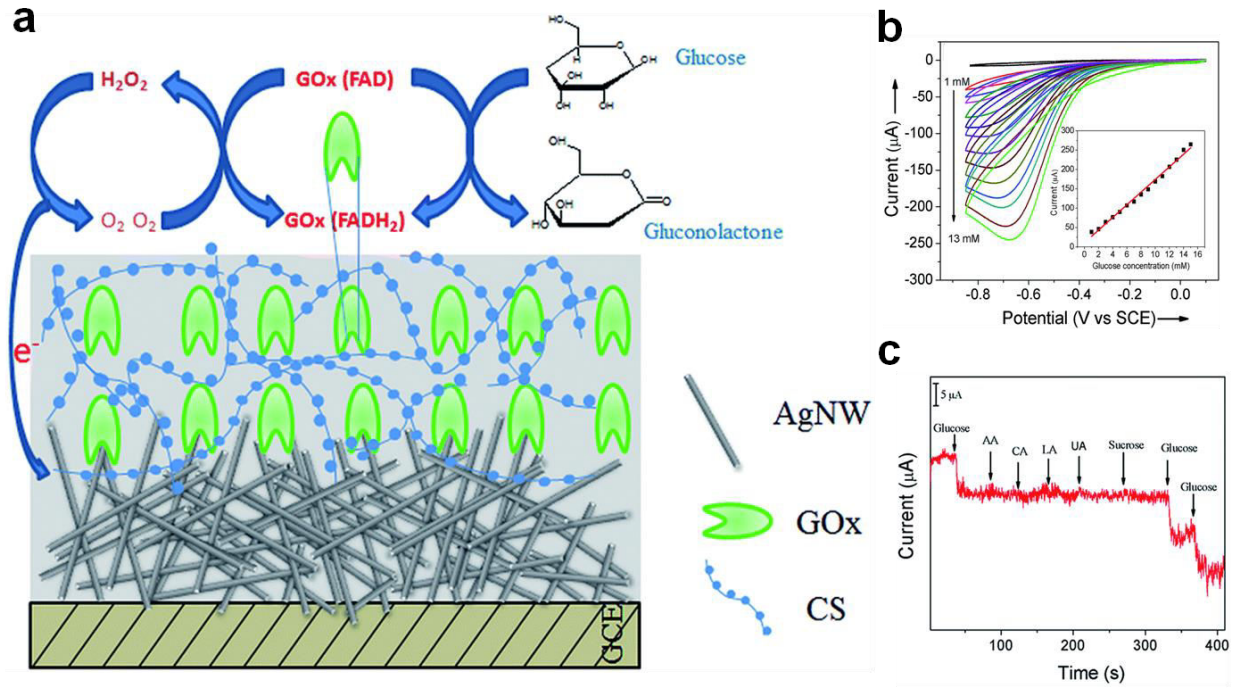

Figure 3. a) Schematic illustration of CS/AgNWs/GOx–GCE modified electrode and the process occurring during the enzymatic electrochemical glucose sensing. b) Cyclic voltammograms of CS/AgNWs/GOx–GCE in 0.1 M PBS (pH 7.4) with successive addition of glucose. The inset shows the calibration curve. c) The amperometric response is showing the effect of interfering substances (1 mM of acetic acid, citric acid, lactic acid, uric acid, sucrose, and glucose, respectively).[64] Reproduced from Krishman-Kumar, S.; Chakaravarthy, S.; Hernandez-Rangel, A.; Prokhorov, E.; Luna-Barcenas, G.; Esparza, R.; Meyyappan, M. RSC Advances 2016, 6, 20102-20108 (ref 64), with permission of The Royal Society of Chemistry.

Another enzyme-based amperometric sensing platform for glucose detection was reported by Deng and coworkers.[65] The authors electrochemically polymerized *m*-dihydroxybenzene (mDB) onto the surface of a GCE in the presence of graphene oxide (GO) to obtain a GO/P*m*DB composite, which was later used to immobilize GOx. The obtained composite was electrochemically reduced to RGO/P*m*DB by application of a negative potential.

The electrode modified by the composites exhibited excellent electrocatalytic activity towards the oxidation of H_2O_2 owing to the synergistic effect of RGO and PmDB. As a result of the high electrocatalytic activity towards H_2O_2 oxidation, the composites were further coated with a Nafion membrane and immobilized with GOx for determination of glucose concentration. By monitoring the oxidation peak current change upon glucose addition at constant O_2 concentration, a calibration curve was obtained with the linear range from 0.5-15 mM, and a LOD of 0.023 mM. In addition, the biosensor was also shown to be selective in the presence of common interfering species.

Electrochemical-based enzymatic glucose sensors generally suffer from signal drift due to the reaction instability in vivo. The electroactive interferences in real blood samples are also a potential concern. Alternatively, optical-based glucose sensors have attracted significant attention because they can be fabricated as label-free, and continuously monitor blood glucose concentration in a real-time fashion. Recently, Yetisen *et al.* reported phenylboronic acid hydrogel-modified optical fibers for continuous glucose monitoring.[66] The hydrogel-based optical fibers were composed of a poly(acrylamide-co-poly(ethylene glycol) diacrylate-co-3-(acrylamido)-phenylboronic acid) p(AM-*co*-PEGDA-*co*-3-APBA) core and a Ca^{2+} crosslinked alginate cladding as shown in Figure 4a. The hydrogel optical fiber core was prepared by injecting the monomer solution into a commercial poly(vinyl chloride) (PVC) tube and polymerized under UV irradiation; the diameter of the core was defined by the inner diameter of the PVC that was varied from 200 μm to 2.0 mm. By immersing the resultant core in sodium alginate solution, a thin cladding hydrogel layer could be added onto the core upon exposure to $CaCl_2$ solution. The core and cladding layer can be visualized via fluorescence imaging as shown in Figure 4f. The optimized hydrogel fiber with p(AM-co-PEGDA) (97:3 mol %) showed ideal

flexibility (Figure 4e) and mechanical properties with tensile strain up to 0.74 mm mm^{-1}. The diol group in glucose can bind to the APBA moiety in the fiber's hydrogel core, which results in an osmotic pressure increase that led to hydrogel fiber swelling and ultimately affected the light propagation through the fiber as demonstrated in Figure 4b-d. Thus, glucose concentration can be quantified by measuring the change in light transmission through the fiber, as shown in Figure 4h. In addition, the authors demonstrated that the hydrogel optical fibers exhibit fast response times, specifically 17-fold higher than what is required. The potential error induced by the presence of interfering biological species was investigated and showed negligible impact, e.g., , fructose and lactate (less than 1%), Na^{+} (-1.435%), K^{+} (-0.097%), Ca^{2+}(-0.002%) and Mg^{2+}(-0.023%). Interestingly, by injecting the hydrogel optical fiber into a desired location of biological tissue as shown in Figure 4g, a real-time in vivo optical glucose sensor could be generated.

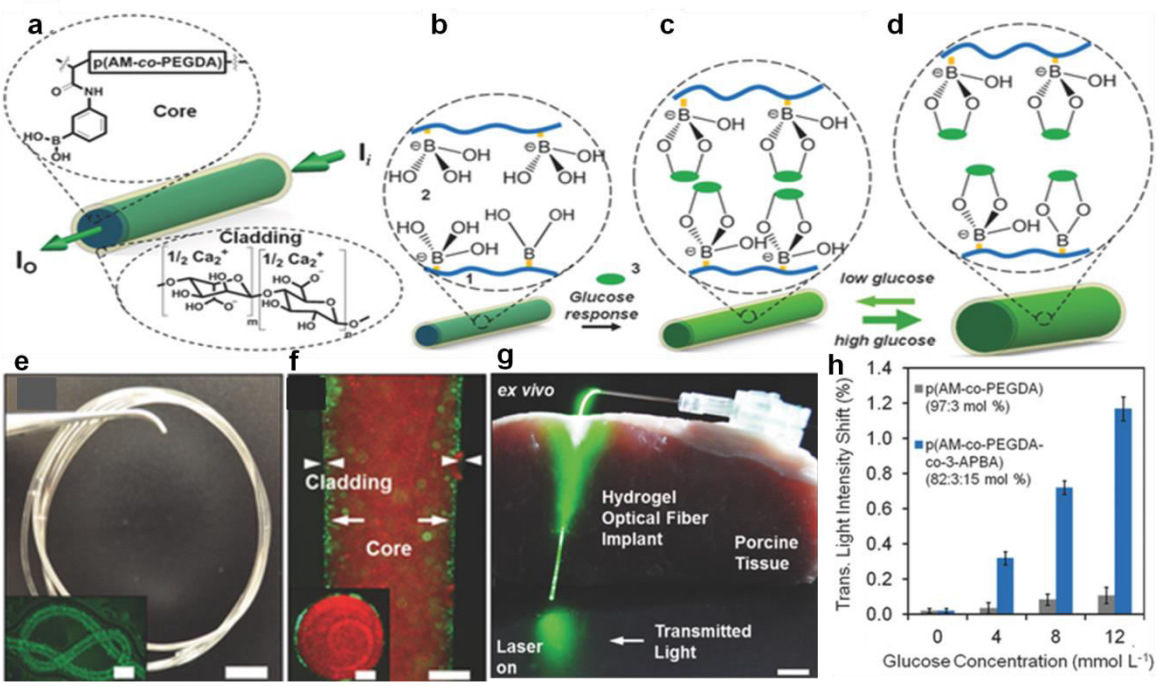

Figure 4. a) A schematic illustration of hydrogel optical fibers composed of p(AM-co-PEGDA-co-3-APBA) core and Ca alginate cladding. b) 3-APBA functionalized hydrogel matrix. (1) PEG-crosslinked polyacrylamide hydrogel; (2) charged tetrahedral state of 3-APBA; (3) glucose. c) Glucose-APBA binding complex with hydrogel fiber diameter change. d) Glucose concentration induced hydrogel swelling/deswelling conformational change and associated with output light intensity changes. e) Photograph of the fabricated optical hydrogel fibers. Scale bar 5 mm. The inset fluorescent image of hydrogel fiber knot doped with green fluorescent beads with scale bar of 500 µm. f) a fluorescence image of hydrogel fibers with red fluorescent dye labeled core and green fluorescent dye labeled cladding. Scale bar 500 µm. The inset image represents a cross section of hydrogel fiber with scale bar of 200 µm. g) Transmitted light intensity change as a function of glucose concentration of p(AM-co-PEGDA) (gray) and p(AM-co-PEGDA-co-3-APBA) (blue) composed hydrogel fiber.[66] Reproduced from Glucose-Sensing Hydrogel Optical Fibers Functionalized with Phenylboronic Acid, Ali K. Yetisen, Nan Jiang, Afsoon Fallahi, Yunuen Montelongo, Guillermo U. Ruiz-Esparza, Ali Tamayol, Yu Shrike Zhang, Iram Mahmood, Su-A Yang, Ki Su Kim, Haider Butt, Ali Khademhosseini, Seok-Hyun Yun, Advanced Materials, Vol. 29, Issue 15 (ref 66) Copyright 2017 Wiley.

Asher and coworkers developed a photonic crystal hydrogel-based sensor for glucose detection.[67] Here, the authors fabricated a glucose/galactose binding protein (GGBP) hydrogel containing non-close packed photonic crystals (PC) attached to a surface. GGBP selectively binds to D-glucose and D-galactose that leads to a conformational change of the GGBP protein and triggers the hydrogel volume phase transition (VPT). The induced VPT upon protein-ligand recognition shrinks the hydrogel and decreases the PC particles spacing that leads to color change due to the light diffraction shift within the PC structure. The technology quantitatively

detected glucose over a concentration range of 0.2μM to 10 mM with a LOD of 1.5 x 10^{-7} M. Furthermore, the 2D PC-GGBP hydrogel sensor showed to be highly selective towards glucose and reversibility during 10 cycles of glucose exposure.

2.3.2 Hydrogen Peroxide

Hydrogen peroxide (H_2O_2) is an important intracellular signaling molecule especially in the regulation of many physiological processes and is a byproduct of many metabolic processes in living organisms. Excess concentrations of H_2O_2 in the human body would result in severe damage for cells and dysfunction of proteins/DNA, thereby leading to various autoimmune diseases, neurodegeneration, and cancer.[5, 68-69] Therefore, selective detection of H_2O_2 in a clinical setting is of importance. To overcome limitations involved in H_2O_2 sensing strategies when using enzymatic proteins (such as their inherent instability, limited natural sources and high cost for protein purification) as well as the low efficiency of most nanomaterials that show peroxidase-like activities, Qiu and coworkers developed coordinated polymer nanoparticles (CPNs) that act as nanozymes using cerium (Ce(III)) and ATP in Tris-HCl buffer for selective H_2O_2 detection.[70] The ATP molecule serves as bridging ligand and the Ce provides photoelectric properties to the obtained CPNs. In the presence of H_2O_2, the fluorescence ATP-Ce(III)-Tris CNPs is oxidized to the nonfluorescence Ce(IV)-Tris CNPs. By using this strategy, the authors obtained an LOD down to 0.6 nM.

Fluorescence based-detection strategies have attracted significant attention over various other detection platforms due to their simplicity and fast response times. Zhang and coworkers reported another fluorescence-based approach for the detection of H_2O_2.[71] Here, the authors use a ratiometric fluorescence resonance energy transfer polymeric nanoprobe that possesses dual

fluorescence emission by upon single-wavelength excitation. One of the advantages of using dual-emission fluorescence includes its excellent resistance to interferences, which is not possible with single-emission measurements. The authors fabricated the polymeric nanoprobe by modifying the lipopolymer 1.2-distearoyl-*sn*-glycero-3-phosphoethanolamine-*N*-[amino-(polyethylene glycol)-2000] (DSPE-PEG-NH_2) with two different fluorophores 7-hydroxycoumarin-3-carboxylic acid (HC) and 4-carboxy-3-fluorophenylboronic acid (FPBA). The polymeric nanoprobe was then obtained by self-assembly of the modified lipopolymer into a micelle which was later exposed to Alizatin Red S (ARS) that binds to FPBA. HC is excited at 405 nm and emits at 450 nm while ARS is excited at 450 nm and emits at 600 nm. Upon exposure of the micelles to 405 nm excitation wavelength, the fluorescence spectrum shows a distinct peak at 600 nm. However, in the presence of H_2O_2, deboronation of FPBA occurs leaving it in a non-fluorescent form, causing the intensity at 600 nm to decrease and the intensity at 450 nm to increase. By plotting the fluorescence intensity ratio at 450 to 600 (F_{450}/F_{600}), the authors observed a linear relationship with increasing H_2O_2 concentration with a LOD of 0.76 μM and limit of linearity up to 500 μM.

Serpe and co-workers reported a novel H_2O_2 sensing strategy using microgel-based optical devices known as etalons.[68] These optical devices have fascinating chemical and physical properties such as easy signal readout, which can be monitored by visual color change, easy operation, and low-cost.[72-74] The authors fabricated the optical devices by sandwiching ferrocene-modified poly(N-isopropylacrylamide)-co-acrylic acid microgels (FE-pNIPAm) between two thin gold layers that act as mirrors. When light strikes the device, it undergoes constructive and destructive interference within the etalon's microgel-based cavity that results in a visual color due to selective reflectance of certain wavelengths of light. It is well known that

for these devices the wavelength of light reflected depends primarily on the distance between the two gold mirrors as shown in Figure 5. As the microgels shrink, the distance between the two gold mirrors decreases, leading to a blue-shift in the peaks in the reflectance spectra. The resultant microgels and etalons were found to respond to H_2O_2 exposure by shrinking in a manner that depended on H_2O_2 concentration. This was attributed to the interaction of the polar amide groups of the microgels with the positively charged (+1) ferrocene. They found that the response to H_2O_2 concentration was linear in the range of 0.6−35 mM and that H_2O_2 generated from biological enzymatic reactions such as in the case of glucose oxidation by glucose oxidase could be detected using this strategy.

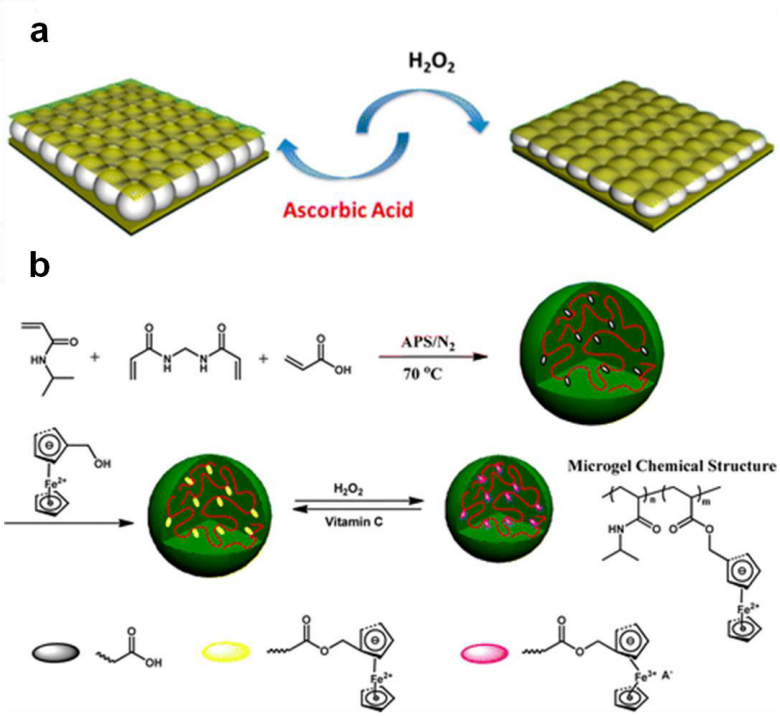

Figure 5. a) A schematic illustration of etalon structure and H_2O_2 sensing mechanism. In the presence of H_2O_2, the distance between the two gold layers decreases and leads to a blue-shift in the peaks of the reflectance spectra. The peaks in the reflectance spectra return to their original position upon exposure to ascorbic acid. b) Microgel synthesis scheme and resulting microgel

chemical composition.[68] Reproduced from Zhang, Q. M.; Berg, D.; Duan, J.; Mugo, S. M.; Serpe, M. J. ACS Applied Materials and Interfaces 2016, 8, 27264-27269 (ref 68). Copyright 2016 American Chemical Society.

2.3.3 Urea

Urea is one of the elementary metabolites found in living organisms and is a vital biomarker for potential kidney malfunction.[60, 75] Therefore, estimation of urea levels in human serum and urine is crucial for diagnosis of liver and kidney maladies. Most of the detection approaches for electrochemistry-based urea sensors involves two enzymes (urease and glutamate dehydrogenase) and a mediator for electron transfer. Generally, the urea can be hydrolyzed into ammonium and carbonic ions in the presence of urease, while the generated ions would be captured by the second enzyme. In the mean time, the electron was transferred to the electrode to produce a signal by the mediator.

Das *et al.*[76] reported a novel urease-conducting polymer hydrogel membrane (CPHM)-modified GCE electrochemical sensor for urea detection. To generate the CPHM, a non-conducting hydrogel film was first polymerized on the GCE at 40-45 ℃ by dropping a preheated solution of monomer (acrylamide 15% and PVA 2.5%), crosslinker (glutaraldehyde 12.5%) and initiator (potassium peroxodisulfate) on the electrode tip. The conducting component, polyaniline (PANI), was doped into the hydrogel network by electropolymerization in an aniline solution. Finally, urease was immobilized covalently into the CPHM network utilizing glutaraldehyde, which can react with the amino group in urease and PANI. The obtained urease-CPHM modified GCE electrode was applied as a working electrode in a three-electrode electrochemical cell. It is well known that the conductivity of PANI is strongly dependent on its electrochemical state, and

hence solution pH. Specifically, the conductivity of PANI is high in acidic solution while it decreases as the solution pH increases, which will in turn lead to an increase in the reduction current. In this system, the solution pH is greatly dependent on the amount of urea that is hydrolyzed by urease because the reaction generates ammonium hydroxide. As a result, the reduction peak current varied in proportion to the concentration of urea in solution. The sensor provided good linearity over a range of urea concentrations (1.5–1000 mM), a high sensitivity of 878 mA mM^{-1} cm^{-2} and a low detection limit of about 60 nM.

As was mentioned above, the hydrolysis of urea by urease generates ammonium hydroxide that increases solution pH. Therefore, other detection platforms that require minimal instrumentation to measure solution pH have been generated. For example, Yang and coworkers reported an inverse opal photonic crystal polymer (IOPP) film for urea detection.[77] The 3D-ordered IOPP film was synthesized by polymerizing methacrylic acid (MAA) in the presence of silica nanospheres (220 nm diameter) using the crosslinker ethylene glycol dimethylacrylate under UV irradiation. The silica hard sphere template was locked into the 3D polymer network in the process of polymerization, which left multiple voids after their dissolution in HF solution. The ordered 3D void structure exhibited allowed specific wavelengths of light to be reflected due to light interference in the photonic material. In addition, the Bragg diffraction peak shift is dependent on the distance between each void, which can be tuned by solution pH. Thus, the carboxylic groups in the polymer matrix can be deprotonated when solution pH increases above MAA's pKa, resulting in an osmotic pressure increase, repulsion between the negative charges in the polymer network and ultimately its swelling. The swelling will increase the distance between the voids yielding a red shift of the Bragg peak. Therefore, the IOPP film is hypothesized to show a red-shift of the Bragg peak in the presence of urea that should increase as the amount of

urea in the system increases. Interestingly, in this colorimetric assay, the urease was not incorporated in the hydrogel film and was added directly in the test solution, which eliminated the complex immobilization process that was required for general biosensor fabrication. The IOPP film showed a pronounced green to red color change as urea concentration increased from 0 to 50 mM with negligible interference from other species like formamide, methylurea and 1,3-dimethylurea. In addition, this sensor can be reused multiple times without obvious loss in performance.

Chaudhari *et al.* reported the development of single fluorophore and dual fluorophore ratiometric biosensors based on fluorescein-iso-thiocyanate-dextran (FD)/FD-Urease encapsulated alginate microcarriers for pH and urea analysis in urine samples.[78] They utilized air driven atomization for layer-by-layer self-assembly of polyallyl amine hydrochloride (PAH) and polystyrene sulfonate (PSS) in conjunction with Tris(bipyridine)ruthenium(II) chloride (RuBpy) forming PAH-PSS (RuBpy)-PAH over FD/FD-Urease loaded alginate microspheres to form FD loaded alginate microspheres (FDAM) and FD-Urease loaded alginate microspheres (FUAM). This led to the formation of a ratiometric pH sensor (RDAM) and a ratiometric urea sensor (RUAM). The FD and RuBpy served as indicator and reference fluorophores, respectively, and urease served as the biological recognition element, which catalyzes the conversion of urea into ammonium hydroxide ions. The alkalinity generated in the microenvironment due to the catalytic reaction causes an increase in fluorescence emission at 520 nm. Use of FD (λ_{ex} 488 nm and λ_{em} 520 nm) and RuBpy (λ_{ex} 488 nm and λ_{em} 610 nm) in a matrix enables single excitation and dual emission ratiometric sensing. In the case of urea measurement, urine samples were diluted ~20 times and the resulting solution was used for spiking different concentrations of urea (0–100 mM). FUAM and RUAM (100 μL) particles were exposed to urea concentrations in the range of

0–50 mM (10 μL) and volume made up to 1.5 mL with Milli-Q water. Fluorescence emission scans were captured (λ_{ex} 488 nm, λ_{em1} 520 nm, λ_{em2} 610 nm). The intensity ratios of I_{520}/I_{610} were plotted against the different urea concentrations. The proposed strategy was able to detect urea up to 50 mM in samples over the pH range of 6-8.

2.4 Body Temperature Sensors

Temperature control is one of the key factors in homeostasis and multiple other biological processes. Body temperature varies both spatially and temporally in an effort to transfer heat between the body and the environment. Furthermore, temperature affects the rate of various biochemical reactions involved in physiological activities. Accurate measurement of localized temperature changes in soft tissue regardless of large-scale motion is also critical in understanding the phenomena of homeostasis, and to assess various medical conditions, such as cardiovascular diseases, pulmonary diagnosis, and other syndromes[79-81] and further offer possibilities of building a smart healthcare and medical system.

Numerous sensor devices have been realized to detect temperature through certain physical changes, including resistive temperature detectors,[82] thermally sensitive resistors,[83] mercury thermometers, infrared sensors,[84] thermocouple sensors,[85] field-effect transistors,[86] optical sensors,[87] as well as luminescent materials.[88] A wide variety of materials have been applied to fabricate temperature sensors, such as carbon-based materials,[89] metallic particles,[90] polymeric materials,[91] and their composites.[92] Among these, polymers with desirable qualities have contributed immensely to the advancement of temperature sensor development. For example, temperature sensors consisting of Ni microparticle doped semi-crystalline polymers (polyethylene and polyethylene oxide), were shown to exhibit high sensitivity for monitoring

human body temperature.[93] The thermal behavior of the polymer was shown to have a great impact on the resistivity. That is, when the polymer transitions from the crystalline phase to amorphous phase a large volume expansion is observed. The expansion led to an increase of the Ni microparticle interparticle distance, which ultimately affect the corresponding conductivity.

Wearable sensors have become increasingly popular as the desire to continuously monitor health and wellness persists. Wearable sensors are challenging to develop as they typically need to be attached to skin, and parameters need to be monitored and reported in real time often when a person is in motion.[15] Furthermore, to realize scalable designs for multipoint tests on moving human subjects, new demands for interconnections with mechanical stretchability on an elastic substrate is essential to withstand sudden impact or large deformation of the human skin. These sensors are mainly separated into two categories. One approach is to dope functional materials into a polymer matrix to form conductive composite materials.[80, 94] The advantage of this approach is high sensitivity but these sensors often only operate over a narrow temperature range, are not very accurate, exhibit slow responses, large hysteresis and low stability. The other approach utilizes resistive temperature detectors patterned on polymer substrates.[95] These sensors are far more accurate than the doped sensors and exhibit fast response times and high resolution. However, they are not very sensitive and the electronics required to collect a signal are relatively more complex. Compared to conventional temperature sensors,[96-97] the use of soft and flexible electronics devices[98-100] can reduce mechanical stress induced on the body. They have the ability to gather information such as pressure and temperature from dynamic surfaces without impairing the movement or activity of the users. Benefitting from polymeric materials, flexible temperature sensors which gently interface with tissue have been investigated extensively for application in the medical field.

Yokota *et al.*[101] demonstrated orders-of-magnitude changes in electrical properties repeatedly at varying physiological temperatures and conditions using a robust, easy-to-fabricate, flexible temperature sensor based on composites of semi-crystalline acrylate polymers and graphite. Here, changes in the temperature causes a resistivity/resistance change of the polymer matrix that can be detected. This flexible and printable thermal sensor provides high sensitivity of 20 mK and a high speed response time of less than 100 ms, and also large resistance changes near body temperature under physiological conditions with high repeatability (determined 1800 times). With increasing concentration of graphite, the resistivity suddenly decreases to 2×10^4 Ω cm at 10 wt% graphite, which is considered the threshold concentration for percolation conduction, and remains relatively constant above 10 wt%. To ensure the graphite concentration was far above the threshold, 25 wt% graphite was added to polymer matrix for all of the samples in this study. The electrical characteristics of films made of the copolymers with filler are shown in Figure 6a. The sensing temperature, which is defined as the point of maximum slope of the resistivity vs. temperature curve, is moved systematically from 25 °C to 50 °C by changing the mixing ratio. Cyclic stability was evaluated by heating from 29.8 °C to 37.0 °C for 1,800 thermal cycles while monitoring resistivity. The sensors maintain at least a four-order-of-magnitude change in resistivity even after 1,800 thermal cycles, as shown in Figure 6b. Using the same data, resistivity measured at 34 °C, 33.3 °C, and 29.8 °C are plotted in Figure 6c as a function of the number of thermal cycles. Real-time temperature mapping is demonstrated in Figure 6d. When the temperature sensor was touched by a finger, the temperature increased and the current decreased (green and black pixels represent large and small current, respectively). Additionally, these ultraflexible sensors are able to detect small physiological temperature changes. The experimental setup and the device structure is shown in Figure 6e, an ultraflexible sensor with

the total thickness of 38.5 μm was directly placed on a rat's lung and temperature is monitored. Temperature changes of ~0.1 °C were observed with the animal breathing, showing that the temperature sensor could be used for such an application without the sensor causing physical damage to the lung or restricting movement of the lung tissue.

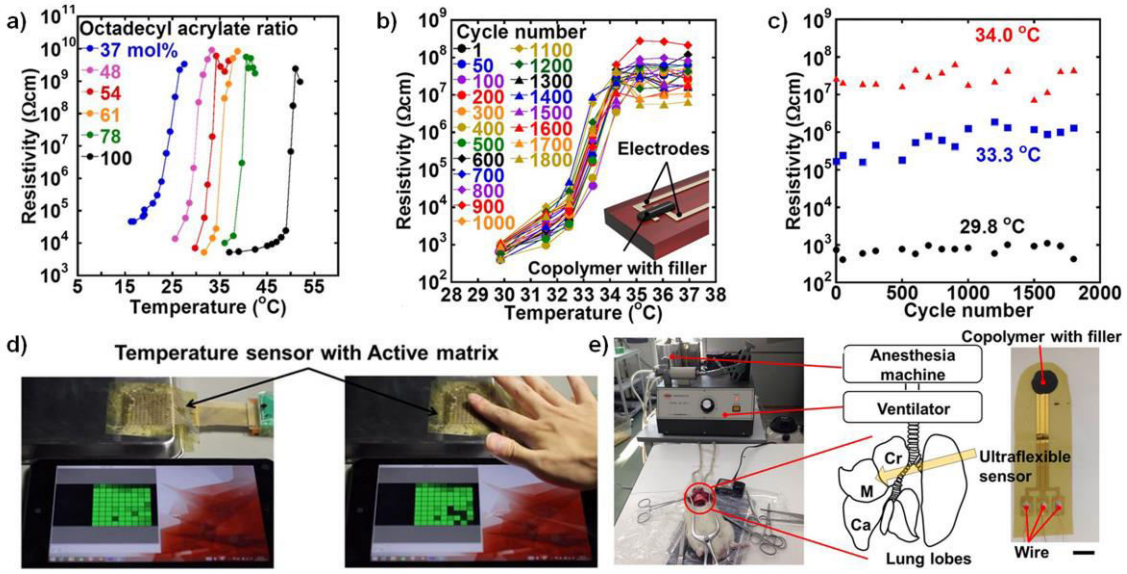

Figure 6. a) Temperature dependence of the resistivity of the copolymer with filler with various comonomer compositions. Control of the sensing temperature of OA/methyl acrylate copolymers with filler is achieved by changing the mol ratio of OA from 37 % to 100 %. b) Heat cycling test for a temperature sensor with 54.0 % OA with a lateral structure. Each cycle comprises two steps: heating from 29.8 °C to 37.0 °C and cooling from 37.0 °C to 29.8 °C. c) The temperature dependence of the resistivity of the temperature sensor with a lateral structure. Black circles, blue squares, and red triangles represent resistance values of 29.8 °C, 33.3 °C, and 34 °C, respectively. d) Real-time measurement of the temperature distribution. (Left) Temperature mapping before touching. (Right) Temperature mapping after touching the sensor sheet with a finger. e) Measurement of lung temperature during respiration, setup of the animal experiments. A median sternotomy was conducted to expose the lung during artificial respiration.[101]

Reproduced with permission from *Proceedings of the National Academy of Science USA* Yokota, T.; Inoue, Y.; Terakawa, Y.; Reeder, J.; Kaltenbrunner, M.; Ware, T.; Yang, K.; Mabuchi, K.; Murakawa, T.; Sekino, M.; Voit, W.; Sekitani, T.; Someya, T. Proc. Natl. Acad. Sci. U. S. A. 2015, 112, 14533-14538 (ref 101).

2.5 Sweat Sensors

Sweating is primarily used to regulate body temperature by cooling the body down with secretion of water. The inability of the human body to sweat properly is potentially harmful, and a complete absence of sweating (anhidrosis) or sweating less than normal (hypohidrosis) in response to heat is also one of the symptoms of some genetic diseases. Additionally, the fact that sweat contains abundant physiological information has been an important driving force for the increasing interests in developing wearable sweat sensors for health monitoring.[102-104] In addition to moisture, sweat is also rich with ions such as sodium, potassium and chloride ranging from 10 to 80 mM.[105] Monitoring sweat's salinity thus provides further useful information. Moreover, sweat may also contain metabolic biomarkers,[106] e.g., glucose, lactate, and uric acid.[107] Sweat analysis is an ideal method for continuously tracking a person's physiological state as it is non-invasive. Currently it is being used for applications such as disease diagnosis,[108] drug abuse detection,[109] and athletic performance optimization.[110] For these applications, the sample collection and analysis are performed separately, failing to provide a real-time profile of sweat content, while requiring extensive laboratory analysis using a variety of analytical tools. While progress has been made in developing sweat sensors,[111] key challenges remain, including lack of being able to monitor multiple things, biocompatibility, and flexibility;, high cost of

manufacturing; and insufficient sensitivity and selectivity. To make improvements in these areas, breakthroughs in materials design and fabrication need to be achieved.

Recently, wearable sweat sensors have been developed using a variety of biosensors to measure analytes of interest. Given the complexity of sweat secretion, simultaneous and multiplexed screening of target biomarkers is critical and requires full system integration to ensure the accuracy of measurements. For example, Davis, Javey and coworkers[112] recently made great progress in this area. They reported a mechanically flexible and fully integrated sensor array for multiplexed in situ perspiration analysis, which simultaneously and selectively measured sweat metabolites (such as glucose and lactate) and electrolytes (such as sodium and potassium ions), as well as the skin temperature (to calibrate the response of the sensors), as shown in Figure 7.

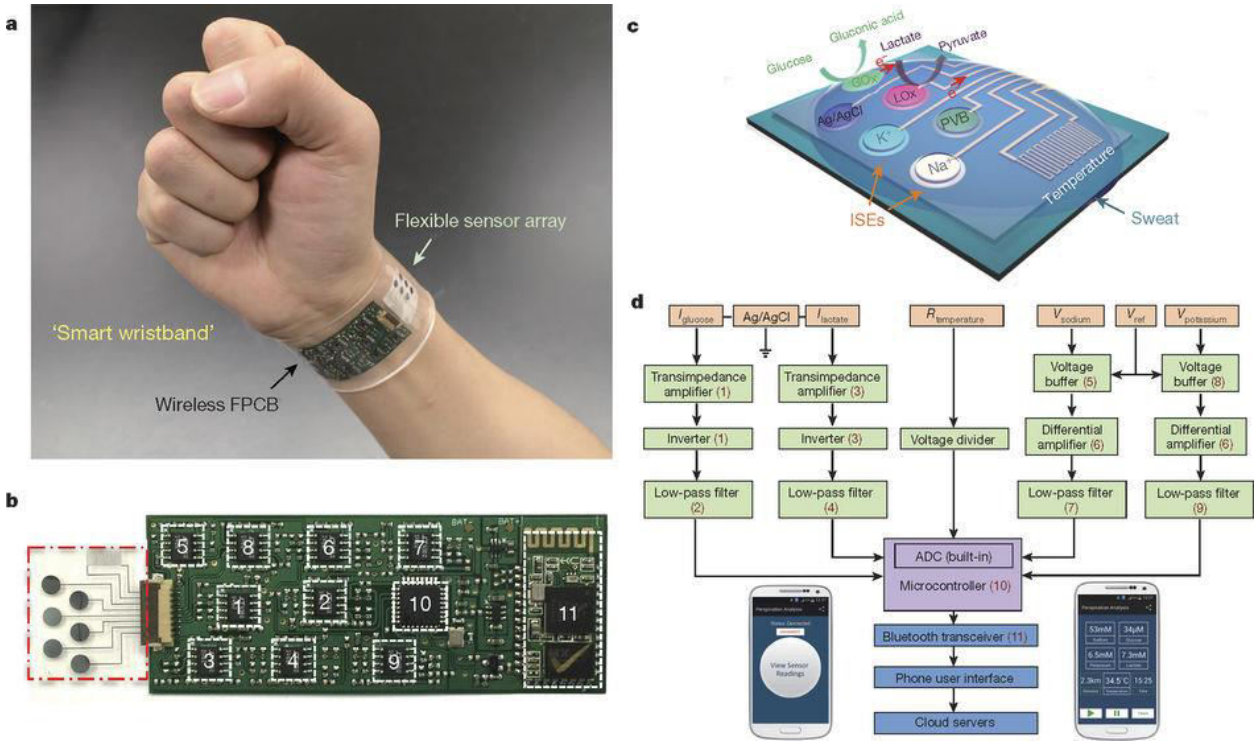

Figure 7. a) Photograph of a wearable flexible integrated sensing array on a subject's wrist, integrating the multiplexed sweat sensor array and the wireless flexible printed circuit board. b) Photograph of a flattened flexible integrated sensing array. The red dashed box indicates the location of the sensor array and the white dashed boxes indicate the locations of the integrated circuit components. c) A schematic illustration of the sensor array (including glucose, lactate, sodium, potassium and temperature sensors) for multiplexed perspiration analysis. Glucose oxidase and lactate oxidase. d) System-level block diagram of the flexible integrated sensing array showing the signal transduction (orange) (with potential V, current I and resistance R outputs), conditioning (green), processing (purple) and wireless transmission (blue) paths from sensors to the custom-developed mobile application (numbers in parentheses indicate the corresponding labelled components in b). ADC, analog-to-digital converter. The inset images show the home page (left) and the real-time data display page (right) of the mobile application. Reproduced by permission from Macmillan Publishers Ltd: NATURE, Gao, W.; Emaminejad, S.; Nyein, H. Y. Y.; Challa, S.; Chen, K.; Peck, A.; Fahad, H. M.; Ota, H.; Shiraki, H.; Kiriya, D.; Lien, D.; Brooks, G. A.; Davis, R. W.; Javey, A. Nature 2016, 529, 509-514 (ref 112). Copyright 2016.

As illustrated in Figure 7a, the flexible integrated sensing array allows simultaneous and selective measurement of a panel of metabolites and electrolytes found in human perspiration as well as skin temperature during prolonged indoor and outdoor physical activities. By fabricating the sensors on a mechanically flexible polyethylene terephthalate substrate, stable sensor-skin contact is formed, while the flexible printed circuit board technology is exploited to incorporate the critical signal conditioning, processing, and wireless transmission functionalities using readily available integrated-circuit components. Figure 7c shows the schematic of the

multiplexed sensor array (each electrode is 3 mm in diameter) for sweat analysis, amperometric glucose and lactate sensors (with current output) are based on GOx and lactate oxidase immobilized within a permeable film of the linear polysaccharide chitosan. Figure 7d shows the system-level overview of the signal transduction, conditioning, processing, and wireless transmission paths to facilitate multiplexed on-body measurements. The signal-conditioning path for each sensor is implemented with analog circuits and in relation to the corresponding transduced signal. The circuits are configured to ensure that the final analog output of each path is finely resolved while staying within the input voltage range of the analog-to-digital converter.

The independent and selective operation of individual sensors is preserved during multiplexed measurements by employing highly specific surface chemistries and by electrically decoupling the operating points of each sensor's interface. This platform is a powerful tool with which to advance large-scale and real-time physiological and clinical studies by facilitating the identification of informative biomarkers in sweat.

Finally, it is critical to develop sensors for human health monitoring that are sensitive to various analytes in a variety of biological media (e.g., blood, saliva, and urine) that can contain important molecular biomarkers to monitor human health. While many polymer-based sensors have already been developed, they are usually a passive element in the sensor that simply allows analyte binding to be converted to a readable signal. To access more advanced sensors, researchers have pursued stimuli-responsive polymers to develop "smart sensors". For example, temperature responsive polymer-based materials (e.g., PNIPAm) can change their physical properties in response to small variations in temperature. Many other stimuli-responsive

polymers are available that can be used as active elements in sensing technologies that were not detailed here, although their use in human health monitoring devices is very promising.

3. Food and Waterborne Pathogen Detection

The detection of bacterial pathogens such as *Salmonellae*, *Vibrio*, *Shigella*, *Escherichia (e.g., E. coli)*, *Staphylococcus*, and *Yersinia*, is extremely important to identify early stages of infection to prevent transmission in a population to control outbreaks, as well as to start treatment as early as possible. This has become especially important with the increased number of infections by multidrug-resistant bacteria.[113-114] With technological progress, various approaches have been developed over the past decade to overcome the limitations of traditional phenotypic identification methods in terms of increased sensitivity, selectivity and reduced analysis time. Some of these approaches include real time polymerase chain reaction (real time PCR), matrix assisted laser desorption ionization-time of flight mass spectrometry (MALDI-TOF MS), and immunological assays such as ELISA.[115-116] Although these methods can provide reliable results, with a very low LOD, they are costly and can be time-consuming. In addition, these approaches require the use of laboratory facilities and skilled technical staff, which limits their application for point-of-care (POC) diagnostic applications. Thus, the development of low cost, easy to use sensing platforms for pathogenic bacteria is drawing a lot of interest.

Depending on the type of sample that needs to be analyzed for the presence of bacteria, different requirements for dynamic range, sensitivity and minimum detectable bacterial concentration is needed. For instance, the Canadian Drinking Water Quality Guideline for *E. coli* is none detectable per 100 mL.[117] On the other hand, clinically relevant bacteria concentrations in the bloodstream and on skin are 10^0-10^4 and 10^2-10^6 CFU mL^{-1}, respectively.[118] In addition,

when detecting DNA from samples containing low bacteria concentrations, the sensing technology needs to be capable of detecting femtomolar concentrations, which is extremely challenging. Thus, detection of the whole bacteria, instead of molecular signatures of the bacteria, carries certain advantages.

Polymeric materials are attractive candidates for the development of functional interfaces and sensing platforms. For instance, researchers have been using hydrogel scaffolds for wound dressings, tissue engineering, and contact lenses due to their advantageous properties, which we already mentioned above.[119-121] These materials in direct contact with biological systems can provide early insights into contamination or infection. Schonherr and coworkers developed a self-reporting wound-dressing platform for the detection of *E. coli* using chitosan hydrogels.[122] These materials work by detecting enzymes (e.g., β-glucuronidase (β-GUS)) that are secreted by bacteria; β-GUS is secreted by 98% of all known *E. coli* strains. The chitosan modification and enzyme detection scheme can be found in Figure 8. The chitosan hydrogel was modified with the fluorogenic substrate 4-methylumbelliferyl-β-D-glucuronide (MUG) and the chromogenic substrate 4-nitrophenyl-β-D-glucuronide (PNPG) that are hydrolyzed by β-GUS presented in *E. coli* medium, generating the infection-reporter dyes 4-methylumbelliferone (4-MU) and 4-nitrophenol (4-NP), respectively that change the color of the wound dressing. The advantage of using both fluorogenic and chromogenic substrates is that one can visualize the color change of the hydrogel by eye and/or upon exposure to UV light. The authors couldn't use this strategy to quantify the concentration of bacteria as the production of β-GUS was highly dependent on the environment and nutrients available for the bacteria. However, the self-reporting chitosan hydrogel showed a LOD for β-GUS of 40 nM when monitoring 4-NP and <1 nM when monitoring 4-MU for an observation time of 15 min. Although the self-reporting hydrogel

platform does not differentiate between *E. coli* strains, using this technology, diagnostic processes can be shorten as only *E. coli* differentiation procedures will be required.

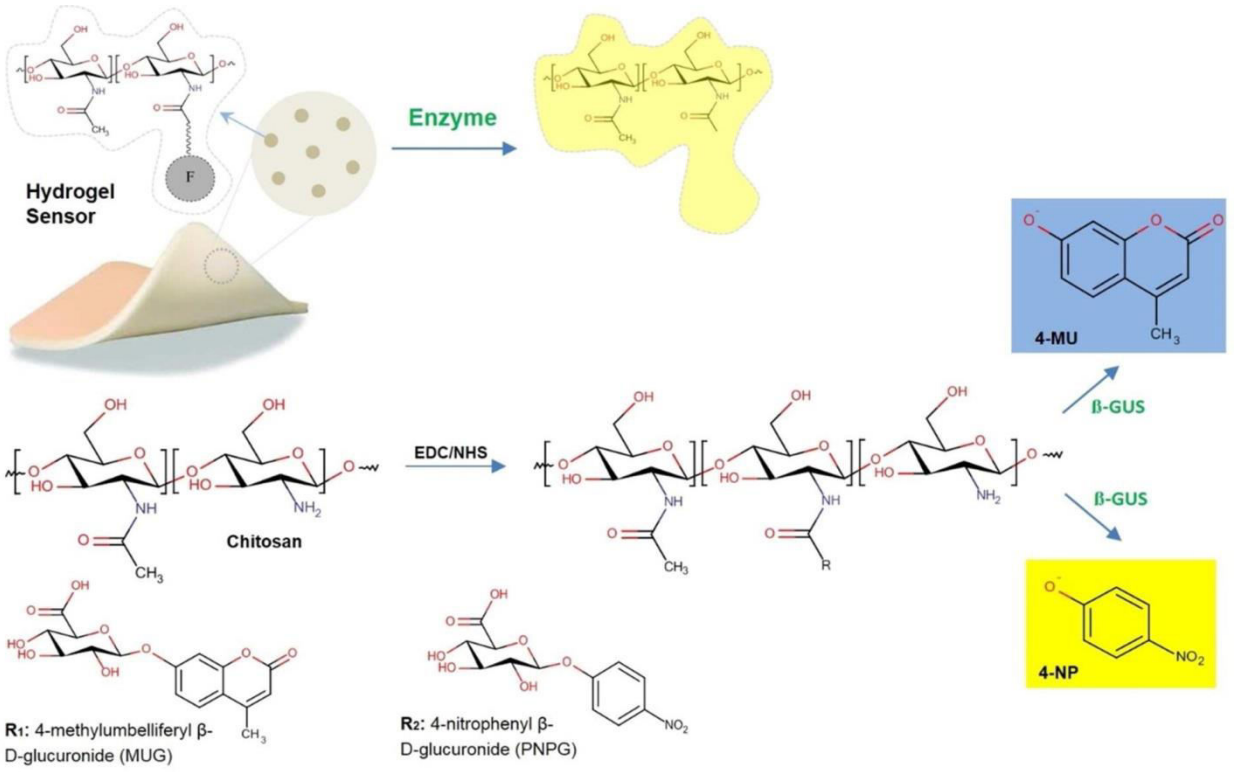

Figure 8. Representation of the enzyme-sensing hydrogel platform and modification details of the chitosan hydrogel. After hydrogel modification with MUG and PNPG, *β*-GUS secreted by bacteria can interact with the hydrogel and produce 4-NP ad 4-MU.[122] Reproduced from Ebrahimi, M. S.; Voss, Y.; Schonherr, H. ACS Applied Materials and Interfaces 2015, 7, 20190-20199 (ref 122). Copyright 2015 American Chemical Society.

Conducting/conjugated polymers have also attracted significant attention in the development of chemical- and bio-detection strategies due to their high electrical conductivity, low cost, and good processability. For instance, Sheikhzadeh *et al.* developed an impedimetric biosensor using a poly(pyrrole-co-3-carboxyl-pyrrole)-aptamer conjugate (aptasensor) for *Salmonella Typhimurium (S. Typhimurium)* detection.[123] The electrochemical approach relies on

the high affinity and specificity of the aptamer for *S. Typhimurium*, and does not use redox probes, like the other examples presented in this review. In this case, the binding of the bacteria and aptamer changes the measured impedance, which depends on the concentration of *S. Typhimurium* over the range of 10^2-10^8 CFU mL^{-1}. This sensor exhibited a LOQ of 10^2 CFU mL^{-1} and LOD of 3 CFU mL^{-1}. In addition, the sensor exhibited good reproducibility, with an average relative standard deviation (RSD) of 5.2% for 3 repeated experiments using 3 different aptasensors. The selectivity of the electrochemical device was also tested against *E. coli* (three different strains), *Enterobacter* and *Citrobacter* in 100 mM $LiCO_4$ solution, which showed much lower relative resistances for these 5 bacteria than those measured for *S. Typhimurium.* The authors further showed that the sensor could be used to detect *S. Typhimurium* in apple juice in 45 minutes.

In a another example, Leong and coworkers reported a novel electrochemical detection strategy for *E. coli* using DNA nanopyramids (DPs).[124] The DNA nanopyramids were thiol modified, which was exploited to immobilize the pyramids onto the surface of a gold-coated substrate with the tip of the pyramid furthest away from the surface being carboxylated and used for the covalent attachment of goat anti-*E. coli* antibodies (Ab). Advantages of using DPs for electrochemical applications include the enhancement of the electron transfer capabilities to the electrode surface due to their unique structure and easy formation of self-assembled monolayers (SAMs) of the thiol-modified DPs on the gold surface. The *E. coli* antibody-modified DPs were used to capture *E. coli* in solution via recognition of the lipopolysaccharides (LPS) antigens found on the bacterial wall surface. Next, a ferrocene-tagged secondary antibody was added to the system, which could bind the bacteria, forming a sandwich; the redox tag could then be

detected electrochemically. By using this strategy, the authors achieved a LOD of 1.20 CFU mL^{-1} and 0.20 ng mL^{-1} of LPS when using a cell lysate sample.

The ability of cationic polymers to bind specific bacteria has also been investigated for the development of pathogen detection strategies. Cationic polymers interact with bacteria through electrostatic and hydrophobic interactions and the strength of the interactions is dictated by the bacterial wall surface structure. Thus, because different bacteria have different surface compositions, they will interact with these polymers with different strengths that can lead to differentiation between bacterial strains. In one example, Wang and coworkers explored the ability of cationic conjugated poly(fluorine-co-phenylene) (PFP-NMe_3^+) modified with cucurbit[7]uril (CB[7]) to discriminate between pathogens and subsequently develop an optical sensor for the simple, rapid and in situ detection of multiple bacterial pathogens.[125] PFP-NMe_3^+ shows amphiphilic properties and interacts with the pathogen's negatively charged membrane by electrostatic *and* hydrophobic interactions. Upon the formation of the fluorescent complex PFP-NMe_3^+-CB[7], the hydrophobic interactions are less favorable as CB[7] buries the hydrophobic side-chain alkyl groups. Therefore, characterizing the interaction of PFP-NMe_3^+-CB[7] with a particular pathogen, and comparing it to the interaction of PFP-NMe_3^+ with the same pathogen after amantadine (AD) is used to release PFP-NMe_3^+ by binding CB[7] to break PFP-NMe_3^+-CB[7] could be used to identify pathogens. Thus, the detection principle is based on recording the fluorescence intensity changes of the conjugated polymer before and after disassembly on the bacterial surface. By using the described assay, which requires 2 h to complete the analysis, the authors could specifically detect different strains of Gram-negative (*E. coli, Pseudomonas aeruginosa*) and Gram-positive (*Bacillus subtilis, Staphylococcus aureus (S. aureus), Enterococcus faecalis*) bacteria as well as fungi (*Candida albicans, Saccharomyces cerevisiae*).

Another detection strategy using cationic polymers for the detection of bacteria in solution (liquid-phase) and in coatings (solid-phase) was reported by Park and coworkers.[126] In this example, the detection of bacteria consists of modifying poly(vinylpyrrolidone) (PVP) with the fluorophore boron dipyrromethane (BODIPY) and using ethyl bromide quarternization to obtain cationic moieties. Upon interaction of the positively charged polymer with the negatively charged surface of the bacteria, fluorescence quenching was observed. After detection, the bacteria could be photothermally-killed by exciting the near-infrared dye IR825 that was covalently introduced into the polymer in the first stage of the polymerization process. This strategy was used to detect *E. coli* and *S. aureus* in solution and was applied as a coating on propylene films for solid-phase detection. *E. coli* showed significant quenching effect on the cationic polymer over *S. aureas* which was attributed to the negatively charged bacterial wall of *E. coli*. For the liquid-phase assay, a minimum concentration of 1 mg/mL of the fluorescent polymer resulted in fluorescence quenching when incubated with 10^8 CFU mL^{-1} whereas for the solid-phase, the minimal detectable bacteria concentration was 10^6 CFU mL^{-1}. The use of free cationic polymer in solution for pathogen detection showed to be very promising although achieving low LODs is still a challenge.

Surface molecular imprinted (SMI) polymers have also been reported as synthetic receptors for the development of bacteria detection platforms. The formation of SMIs typically involves soft lithography or a stamping process that allows the formation of micro- or nano-scaled features on a polymer layer coated on a solid-rigid substrate using a soft polymeric stamp.[127] In an example using SMI, van Grinsven and coworkers reported a detection strategy for *E. coli* and *S. aureus* based on the heat-transfer method (HTM) combined with SMI.[128] The detection strategy consisted of monitoring the thermal resistance across the polymer-solution

interface. The presence of bacteria immobilized on the polymer's surface can block the heat flow through the layer and can lead to a change in the thermal resistance, which was detected based on the input power and the temperature difference between the metal substrate and the solution.[129] Bacterial stamps for *E. coli* and *S. aureus* were prepared with polydimethylsiloxane and were used to imprint the microstructures onto polyurethane layers coated on aluminum chips. Total surface coverage of the imprinted microstructures characterized by using microscopic images for *E. coli* (rod-like shape imprints) was 14.13 ± 1.8 % whereas for *S. aureus* (spherical imprints), it was 12.36 ± 2.3 %. The proposed platform showed to be effective for discriminating dead cells and live cells as well as a high selectivity for *E. coli* when using *E. coli*-surface imprinted polymer. The LOD for the proposed label-free platform was calculated to be 3.5×10^4 CFU mL^{-1} with a maximum detection limit of 2×10^6 CFU mL^{-1}. In order to overcome some of the drawbacks associated with high amount of noise on the thermal resistance signal from the HTM method, which in turn limits the LOD, van Grinsven and coworkers used thermal wave transport analysis (TWTA) combined with surface imprinted polymers (SIP) for the detection of bacteria.[130] In this strategy, the thermal wave propagating through the sample will experience a delay upon bacteria binding to the surface, and the degree of delay depends on the concentration of bacteria present in the system. The LOD for the new strategy was decreased to 1×10^4 CFU mL^{-1} and the sensor platform was able to detect *E. coli* in urine samples at a concentration of 3×10^4 CFU mL^{-1}. Although the detection assay showed very high selectivity against a number of microorganisms in a complex mixture, the detection limit is still far away from what's required for real world applications.[118]

In yet another use of SIPs, Chen *et al*. reported a novel SIP-based electrochemiluminescence (ECL) approach for *E. coli* detection.[131] The authors used *E. coli*

O157:H7 as a template to create microstructures on a polydopamine coated GCE electrode. Polyclonal antibodies against *E. coli* O157:H7 were labeled with graphene quantum dots doped with N (pAb-N-GQD) and used as reporters. Immobilization of the bacteria on the electrode surface leads to the subsequently immobilization of pAb-N-GQDs and generates an ECL signal in the presence of $K_2S_2O_8$ in solution indicating bacterial contamination. As the concentration of bacteria increases on the surface of the electrode, more pAb-N-GQDs can be introduced which further increases the ECL signal intensity. The authors could quantify *E. coli* O157:H7 at concentrations as low as 1×10^1 CFU mL^{-1} and up to 10^7 CFU mL^{-1} with a LOD of 8 CFU mL^{-1}. Furthermore, the authors could detect *E. coli* in water samples that were spiked with different bacteria concentration, showing the potential of this technology for real world applications.

Stimuli-responsive polymers (i.e., smart polymers) respond to their environment by changing their chemical and/or physical properties. Such polymers can be synthesized to respond to a number of external stimuli, such as temperature, pH, humidity, light, electric/magnetic field and biomolecules.[132] The most prevalent applications include drug delivery and biosensing. Rimmer and coworkers reported a bacterial sensing strategy using a highly branched polymer composed of poly(N-isopropylacrylamide) modified with vancomycin (HB-PNIPAM-van), which was able to bind a peptidoglycan within Gram-positive bacteria cell walls.[133-134] The authors observed that visible mats of insoluble aggregates were formed when HB-PNIPAM-van was incubated with *S. aureus* bacteria but no aggregates were formed when HB-PNIPAM-van was incubated with *Pseudomanas aeruginosa*, demonstrating the detection and specificity of the strategy towards *S. aureus*. In addition, they found that for particular bacteria concentrations, the degree of aggregation was dependent on the concentration of the polymer used for incubation. They further compared the behavior of linear and highly branched PNIPAM modified with

vancomycin to detect *S. aureus*. Both polymers were synthesized in a controlled manner to ensure that the amount of vancomycin incorporated on each was the same. Upon incubation of the polymers (5 mg mL^{-1}) with *S. aureus* (10^8 CFU mL^{-1}) for 24 h, it was observed that aggregates were formed for HB-PNIPAM-van while for linear PNIPAM-van no aggregation was observed. This was attributed to the colloidal stability of the polymers. Linear polymers with pendant ligands wrap the vancomycin molecules and shield them from interacting with the bacterial wall whereas branched polymers allow the vancomycin to remain exposed and available for binding.

4. Environmental Pollutant Sensors

Modern industrialization has led to the release of heavy metal/organic contaminants to the environment at unprecedented levels. Therefore, the detection of these species can lead to the early detection of release events, which can lead to early release mitigation activities. For example, it is well known that heavy metal ions are oftentimes found in waste effluents from the mining and tannery industries.[135] The release of these contaminants into the environment has had a significant impact on human health and on various aquatic species due to the non-biodegradability, toxicity, and carcinogenicity of heavy metal ions.[136] Organic aromatics are another kind of environmental pollutants that are mainly produced in the manufacture of pesticides, insecticides, and plastics.[11-13, 137] Newly developed polymer-based assays for the detection of environmental pollutants rely on electrochemistry,[16, 138] fluorescence,[9, 11-13, 139-141] colorimetry[142-143] and UV-vis spectroscopy.[144-146] This section focuses on reviewing recent progress in polymeric material-based technologies for the detection of environmental pollutants.

4.1 Heavy Metal Ions

Mercury is one of the most commonly discussed heavy metal pollutants. The excess mercury ions in water bodies can be converted into methylmercury by aquatic microorganisms, which can potentially be accumulated in the human body through consumption of mercury-contaminated wildlife. Mercury poisoning can lead to serious nervous system dysfunction and illnesses that can ultimately lead to death.[145, 147-148] Vallejos *et al.*[149] recently reported a colorimetric assay for Hg^{2+} detection in fresh fish meat using dithizone (DZ) derivative crosslinked poly(N-(4-aminophenyl)methacrylamide-*co*-1-vinyl-2-pyrrolidinone-*co*-methyl methacrylate) (p(AMA-VP-MMA)) copolymers. The AMA in the copolymer is used for DZ derivative formation and an anchor for internal crosslinking. The other two components (VP and MMA) in the copolymer are used to tune the hydrophobicity of polymers for application in aqueous media as DZ is insoluble in water. The polymer film undergoes a color change from green to red upon exposure to Hg^{2+} due to the formation of the DZ-Hg^{2+} chelate. Thus, the Hg^{2+} concentration can be quantified by measuring the color intensity change via a RGB analysis of a photograph of the film. The reported films exhibited high performance with a fast response (~ 2 min) in the presence of other interferences such as Cu^{2+} and other cations. The feasibility of using the sensor for the detection of Hg^{2+} in fish meat has been demonstrated by observing the sensor film color change after contacting with a fish meat sample. The quantitative results from this colorimetric assay are comparable to those obtained from traditional analytical tools (ICP-MS). The authors claimed that the sensors were reusable at least 10 times. This assay showed a LOD of 1.6 ppb (8 nM) and a wide dynamic range over 5 orders of magnitude (1 nM to 0.1 mM).

A dithioacetal polymer-based chemosensor for Hg^{2+} in aqueous solutions was recently developed by Lee and coworkers.[144] The chemical structure of the dithioacetal polymer (P2 and

P3) is shown in Figure 9a. The polymer solutions exhibited a pale yellow (P2 and P3) to dark red color (P1) change upon exposure to Hg^{2+}, as shown in Figure 9b. In principle, the red color of the azo-derived polymer with aldehyde functionalities in the side chain (P1) (Figure 9a) can be ascribed to the intramolecular charge transfer (ICT) via the push-pull effect of the aldehyde group. After addition of Hg^{2+} to P2 and P3 polymer solution, the dithioacetal group converts to an aldehyde group, which resulted in an irreversible pale yellow to dark red color change, as schematically illustrated in Figure 9c. A maximum 30–40 nm red shift in the UV-vis absorption spectrum can be observed for 24 μM P2 and P3 solutions as Hg^{2+} is added as shown in Figure 9d-1. By measuring the peak shift in the UV-vis absorption spectrum, the amount of Hg^{2+} in solution can be quantified. The response speed of the P2 solution toward Hg^{2+} exposure was shown to be independent of solution pH, while it was decreased from 15 min to 1 min with P3 upon decreasing the solution pH from 7.4 to 3, as shown in Figure 9e. In addition, such polymer solutions (P2 and P3) exhibited good selectivity to Hg^{2+} compared to other alkali and metal ions. The only issue with such a colorimetric assay is the complexity of the polymer synthesis, which involves multiple reactions steps as well as associated purification process.

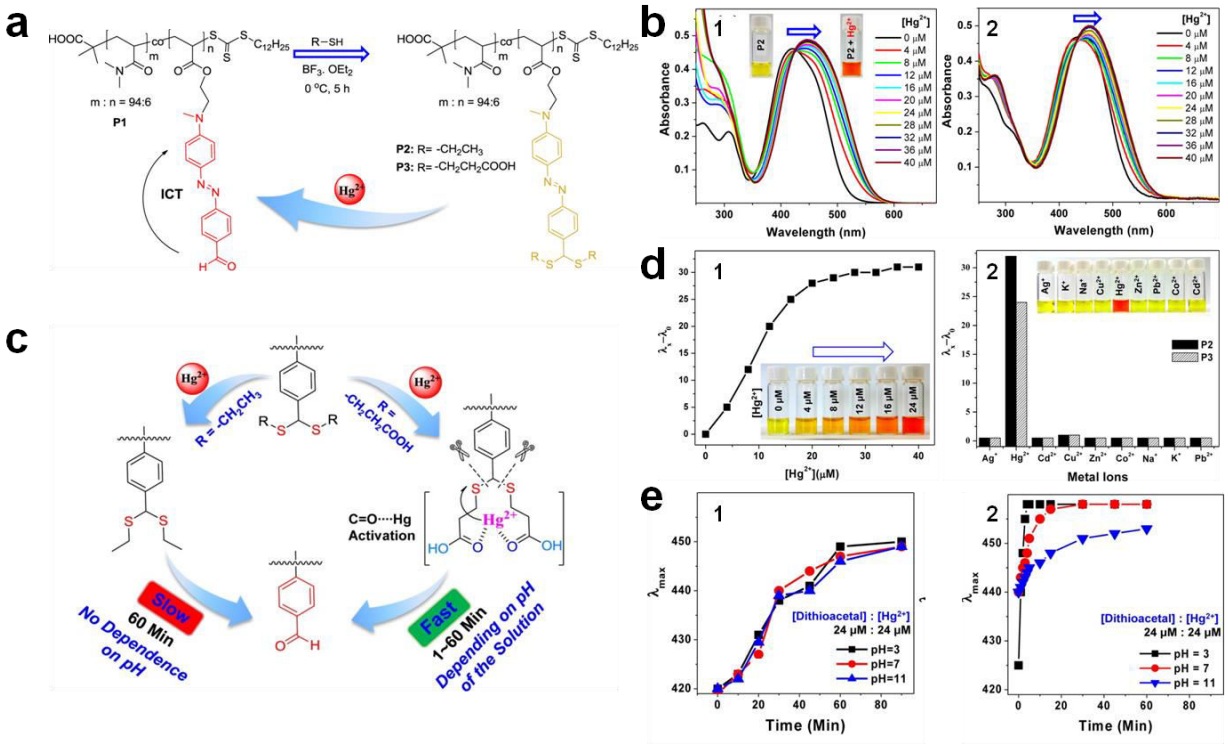

Figure 9. a) Chemically synthesis of Hg^{2+} sensitive dithioacetal polymer. b) UV-vis absorption of 24 μm P2 (1) and 24 μm P3 (2) with different concentration of Hg^{2+} ions in pH 7.4 HEPES buffer. c) Schematic illustration of response speed of P2 and P3 polymers to Hg^{2+} ions and dependence of solution pH. d-1) UV-vis absorbance peak shift of P2 polymer solution as a function of Hg^{2+} ions concentrations. d-2) Selectivity bar diagram of polymers P2 and P3 (24 μm) with various alkali and transition metal ions in HEPES buffer. The inserted photograph is the P2 polymer solution with different metal ions. e) UV-vis absorbance peak shift of a 24 μm P2 (1) and P (2) solution as a function of reaction time in different pH solutions with addition of the same amount of Hg^{2+} ions. Reproduced from Balamurugan, A.; Lee, H. Macromolecules 2015, 48, 1048-1054 (ref 144). Copyright 2015 American Chemical Society.

Copper ions are responsible for controlling multiple physiological processes such as nervous system regulation and are involved in various enzymatic reactions.[150-151] However, Cu^{2+}

species can be toxic at high concentrations.[152] Recently, Ye and coworkers have developed a colorimetric sensor using thiourea modified PVA microspheres for the detection of Cu^{2+} and Hg^{2+}.[145] In this assay, thiourea (chromophore) was attached to the surface of the PVA microspheres resulting in a pale yellow color in solution. After the chromophore bound to Hg^{2+} or Cu^{2+} (1:1 binding), the solution changed color to orange or dark green, respectively. By quantifying the peak shift in the UV-vis spectra, the authors reported a LOD of 0.209 μM and 0.320 μM for Hg^{2+} and Cu^{2+}, respectively; and a linear response up to 10 μM. In addition, the performance of the colorimetric response was not affected in the presence of other cations, such as Na^{+}, K^{+}, Cd^{2+}, Ag^{+}, Co^{2+}, Ca^{2+}, Mg^{2+}, Ba^{2+}, Al^{3+}, Zn^{2+}, Pb^{2+}.

While polymers can serve as a scaffold for modification with analyte reporter molecules, they can also serve to increase the solubility/distribution of analyte reporter molecules in a solution. It has been reported that rhodamine derivatives were able to chelate with metal ions that yields a color change.[153] However, the poor water solubility of rhodamine derivatives restricted their application for metal ion detection in aqueous media. In order to address this shortcoming, Zhou and coworkers recently reported a paper-based colorimetric chemosensor for Cu^{2+} detection. First, the authors synthesized rhodamine B (RhB)-modified poly(ethylene glycoyl) (PEGRh), which increased the RhB water solubility.[142] Upon addition of Cu^{2+} ions, the color of the PEGRh solution changed from colorless to purple with an absorbance peak appearing at 561 nm. The absorbance increased gradually as the Cu^{2+} concentration increased. Thus, a calibration curve can be generated by monitoring the absorbance change at 561 nm as a function of Cu^{2+} concentration. The authors also noted that the fluorescence emission of RhB was quenched after the addition of Cu^{2+} due to the formation of PEGRh-Cu^{2+} complex. In addition, the PEGRh-based chemosensor can work over a wide range of pH from 4 to 10 with a LOD of 25 nM even

in the presence of high concentrations of interfering cations, such as Ba^{2+}, Ca^{2+}, Cd^{2+}, Co^{2+}, Cr^{3+}, Fe^{2+}, Fe^{3+}, Hg^{2+}, K^{+}, Mg^{2+}, Mn^{2+}, Na^{+}, Ni^{2+}, Pb^{2+}, VO^{2+} and Zn^{2+}. Furthermore, the authors showed that the PEGRh could be absorbed by paper, and the color of the paper could be related to the concentration of Cu^{2+} in solution. The selectivity of this paper-based chemosensor has been proven by immersing it into solutions containing various metal ions; a color change is only observed upon exposure to solutions containing Cu^{2+} ions. Finally, the authors showed that the paper-based devices can be used to analyze tap water and river water.

New functionality can be achieved by combining polymers and metal/inorganic nanoparticles (e.g., quantum dots and silica nanoparticles). In one example, Gao *et al.* reported a colorimetric sensor based on poly(vinylpyrrolidone) (PVP) coated Pt nanocubes for Ag^{+} detection.[146] The sensing mechanism is illustrated in Figure 10a. The PVP-capped Pt nanocubes exhibited artificial peroxidase activity and facilitated the oxidation of 3,3',5,5'-tertramethylbenzidine (TMB) by H_2O_2 with a concomitant solution color change. However, in the presence of Ag^{+}, the catalytic activity of the PVP-Pt nanocubes was effectively inhibited and the solution exhibited less color change. The solution color changes were quantified by collecting UV-vis spectra as shown in Figure 10b. By monitoring the absorbance change at 653 nm (maximum absorbance of oxidized TMB, blue color) with and without Ag^{+}, the authors obtained a calibration curve with an LOD of 80 pM Ag^{+} and a linear range of 10^{-2}-10^{-4} nM. Photographs of solutions containing PVP-Pt nanocubes/TMB/H_2O_2 and various concentrations of Ag^{+} is shown in Figure 10c. The color intensity of the solution decreased as the concentration of Ag^{+} increased.

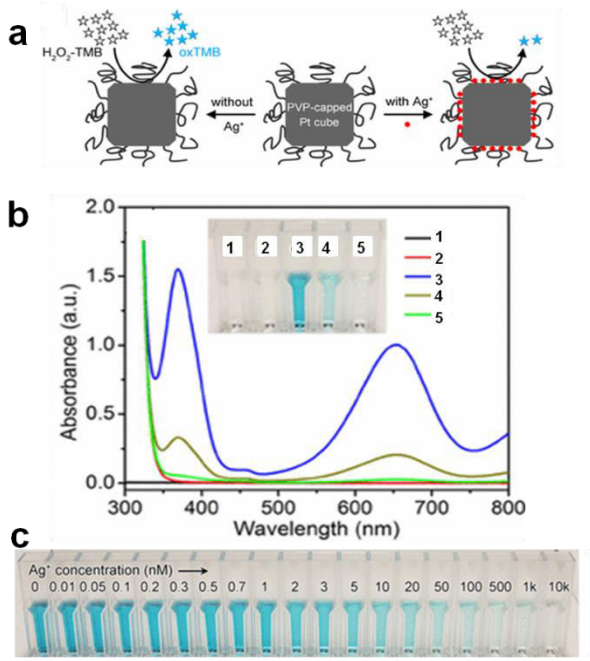

Figure 10. a) A schematic sensing mechanism of colorimetric PVP-capped Pt cubes platform for Ag^+ detection. b) Photographs and corresponding UV-vis spectra of solutions in curettes containing (1) PVP-capped Pt cubes (~3.78×10^{10} particles/mL), (2) TMB-H_2O_2, (3) PVP-capped Pt cubes + TMB-H_2O_2, (4) 50 nM $AgNO_3$ + PVP-capped Pt cubes + TMB-H_2O_2, (5) 10 μM $AgNO_3$ + PVP-capped Pt cubes + TMB-H_2O_2. c) Photographs of reaction solution containing PVP-capped Pt cubes and TMB-H_2O_2 in the presence of different concentrations of Ag^+. Reproduced from Gao, Z.; Liu, G. G.; Ye, H.; Rauschendorfer, R.; Tang, D.; Xia, X. Analytical Chemistry 2017, 89, 3622-3629 (ref. 146). Copyright 2017 American Chemical Society.

4.2 Organic Aromatics

For many years, organic aromatics were released into the environment without proper knowledge of the exact consequences this would have on human and wildlife health and the health of the environment. Many of these compounds are dangerous for humans and wildlife to

contact and consume, and their release into the environment (and in consumer products) needs to be carefully monitored. Compounding the potential danger of certain organic compounds is their poor biodegradability, which allows them to persist for long periods of time, thus allowing them to accumulate. One of the most well-known and well-documented examples of this is the use of dichlorodiphenyltrichloroethane (DDT) as an insecticide in the mid-1940s. Another example is the use of bisphenol A (BPA) to generate polycarbonated plastics and found in beverage bottles and other containers, which could potentially be ingested by humans.[16] BPA is known to exhibit hormone-like properties that can result in unwanted side effects in organisms exposed to BPA. Therefore, BPA use has been banned in many regions around the world for use in drinking bottles and related products. As a result, detection of BPA in samples is vital to identify contaminated products.

In one example, Wang and coworkers recently developed a highly sensitive electrochemiluminescence (ECL) sensor for BPA using a $Ru(bpy)_3^{2+}$/graphen-palladium nanoparticle/polyvinyl alcohol (PdNP-GR/PVA) composite.[137] The $Ru(bpy)_3^{2+}$ was first drop casted onto a polished GCE followed by PdNP-GR/PVA hybrid modification. The ECL effect of $Ru(bpy)_3^{2+}$ was greatly enhanced by the PdNP-GR nanocomposites due to the improved electrocatalytic activity and enhanced electron transfer. The PVA was used as a scaffold to facilitate functional nanocomposite attachment to the electrode that improved the electrode stability and reproducibility. In the presence of BPA, the ECL intensity increased, and a calibration curve for BPA quantification could be achieved by monitoring the ECL intensity at the oxidation peak. A wide dynamic range of 0.1-10000 nM was achieved with a LOD of 0.025 nM. In addition, the sensor exhibit good selectivity in the presence of other cations and nitroaromatics.

MIPs can also be modified on electrode surfaces and used for the selective detection of analytes by exploiting various electrochemical techniques. For example, Advincula and coworkers recently reported an EIS-based BPA sensor using a MIP eletropolymerized on an indium tin oxide (ITO) electrode surface.[16] The MIPs were synthesized by polymerizing two monomers 2-(2,5-di(thiophen-2-yl)thiophen-3-yl) ethanol (G0 3TOH) and 2-(9H-carbazol-9-yl) acetic acid in the presence of the target molecule as a template; it is noted that there is no crosslinker present. The cavities formed throughout the MIPs enhanced the sensing capability and selectivity toward BPA with a LOD down to 0.42 mM. From the cyclic voltammetry scan, the anodic peak current of the MIP-modified electrodes were much higher than non-MIPs modified ones, which means the presence of BPA increased the crosslinking density of monomer and lead to higher current density. In the EIS experiment, the binding of BPA molecules to the MIPs caused a decrease in the electrochemical current by impeding the flow of the electrons in an AC current. As the BPA concentration in solution increased, the radii of the semicircles in Nyquist plots decreased, which indicated that the impedance increased. It can be explained by BPA binding induced electrode surface blocking and extend of blockage is BPA concentration dependent.

Quantum dot (QD)-doped MIP composites have been wildly used for assay development to quantify organic aromatic pollutants in samples.[9, 12, 14, 141, 154] QDs are generally semiconductor particles (e.g., CdS, ZnO, CdTe) with nanometer-scale dimensions. They are ideal candidates for reporter "molecules" owing to their low photobleaching, and narrow and symmetric emission peaks. MIPs generally have the benefit of high selectivity toward target molecules. Therefore, the combination of MIPs and QDs can lead to a highly selective and sensitive assay for aromatic pollutant detection. For example, Li *et al.*[12] recently reported MIP-coated Mn-doped ZnS (Mn-

ZnS) QDs for dibutyl phthalate (DBP) detection, which is a common plasticizer and can be found in water, soil, air and food. The MIPs were synthesized by polymerizing 3-aminopropyltriethoxysilane (functional monomer) and tetraethoxysilane (crosslinker) in the presence of the DBP as the template. Once the DBP was removed from the crosslinked material, a cavity with the molecule shape and H-bonding interactions templated was left behind. Hence the material is hypothesized to have a high affinity for DBP. The detection mechanism is based on the fluorescence quenching of Mn-ZnS QDs in the presence of DBP due to electron transfer. The authors optimized the assay by tuning the ratio of functional monomer and QDs to achieve the highest quenching efficiency. The Mn-ZnS QDs@MIPs nanocomposite-based assay showed a LOD of 0.27 μM DBP with a linear range of 5.0-50 μM.

Trinitrotoluene (TNT) is wildly used as explosive for military, industrial and mining operations. It's a potential hazard for both human health and safety. The overdose consumption (maximum limit is 2.0 ng/mL from Environemntal Protection Agency) of TNT in drinking water can lead to aplastic anemia, toxic jaundice, gastritis, cyanosis, or dermatitis.[155] Uyar and coworkers recently developed a silicon quantum dot (Si QD) decorated Nylon 6,6 nanofiber mat for TNT sensing.[140] The nanocomposites were synthesized by first electrospinning a Nylon 6,6 polymer solution on to aluminum foil and peeled off as a freestanding mat. A dip-coating method was then used to decorate Si QD onto the fibrous polymer mat, which resulted in high fluorescence emission with 400 nm wavelength excitation. Upon exposure to TNT solution, the Meisenheimer complex can be formed between the primary amine on the Si QD surfaces (electron rich) and the TNT aromatic ring (electron poor) due to the donor-acceptor interaction, which led to fluorescence quenching. The quenching efficiency is dependent on the TNT concentration. Thus, a calibration curve for TNT quantification can be achieved by measuring

the florescence intensity changes as a function of TNT concentration. In addition, the complex exhibits a wine-red color under UV irradiation. The Si QD decorated Nylon-6,6 nanofibrous mat remained strongly fluorescent even at extreme pH (2.3 or 12.6). The assay showed high performance with a wide dynamic range of 7.5 nM –1.5 mM of TNT solution. However, the nanocomposites showed slight fluorescence quenching in the presence of 4-nitrophenol, which bring into question the specificity of the sensor.

Generally, the assays mentioned above involved the use of a light source to excite fluorescence, which can limit the applications of the systems. Alternatively, chemiluminescence (CL) can be used, which can light as a result of a chemical reaction and can be used in applications where fluorescence excitation is not possible. In one example, Bagheri and coworkers reported a MIP capped ZnO QD (MIPs@ZnO)-based chemiluminescence (CL) sensor for TNT detection.[154] The MIP layer was synthesized by precipitation polymerization of (3-aminopropyl)triethoxysilane (APTES), which was used as the monomer, and tetraethoxysilane (TEOS) as the crosslinker in the presence of TNT as the template. TNT, as a Bronsted-Lowry acid, showed high affinity toward the amino group of ATPES, which induced chemical templating in the cavities as well as shape templating. In this system, the CL emission of $KMnO_4$-rhodamine B (RB) was enhanced by MIPs@ZnO QDs due to the MIPs@ZnO QDs catalytic activity that facilitated the energy transfer process. Then the CL emission could be effectively quenched by TNT, which can be explained by the formation of Meisenheimer complex between the aromatic ring of TNT molecules and electron-rich amino groups. By measuring the CL quenching efficiency at different concentration of TNT, a calibration curve can be obtained for TNT quantification. In this assay, the MIPs@ZnO QDs itself showed strong fluorescent emission at ~536 nm with excitation wavelength of 389 nm, which can be quenched

by the TNT target binding. Such fluorescent emission of MIPs@ZnO QDs remained constant 50 days after preparation.

Finally, photonic materials that exhibit color due to the material's structure could be use for environmental pollutant quantitation. For these materials, their color (and color change) can be sued to determine the concentration of organic contaminants in solution. Li and coworkers recently reported colorimetric MIP-based photonic sensor arrays for poly-brominated diphenylether detection.[156] A silica colloidal crystal template was first formed by immersing the glass slide in an ethanol solution containing colloidal silica microsphere with good size monodispersity. The precursor polymer solution containing the functional monomer (acrylic acid), template molecules (target), crosslinker (methlenediethylene glycol dimethylacrylate) and initiator was added to a glass slide and pressed into thin layer. Subsequently, a hydrogel layer was formed by exposing the sandwich structure to UV irradiation. Finally, a 3D-ordered macroporous array with imprinted binding sites distributed throughout the macroporous material was created by dissolving the silica colloidal crystal through HF exposure, which left voids and the template sites distributed throughout the macroporous wall. Upon the target binding, it will result in the array periodicity change due to the hydrogen bond formation between target and functional monomer that affects the diffraction properties and lead to ultimately absorbance peak shift. A LOD of pg/g can be achieved by this method.

5. Conclusion and Outlook

The recent work on polymer based technologies for sensor and biosensor has been reviewed with focuses on their applications in human health care diagnosis, food/waterborne pathogen detection and environmental pollution monitoring. The advantages of using polymer

materials for chemical sensing applications are not limited to flexibility, light weight, softness, biocompatibility, stretchability, ease of modification, cost effective manufacturing and long fatigue life. Although significant efforts have been paid to achieve better figure of merit of current sensors, little progress have been seen in commercializing these technology into product that can be used in the real world. The solution for overcoming such challenge is the interdisciplinary collaborations that the chemists developed the sensing scheme, the engineers designed and integrated into compact device, and computer scientist programmed it into a user-friendly fashion.

Biographies

Wildemar S. P. Carvalho is a PhD student under the supervision of Prof. Michael J. Serpe at University of Alberta. He received his B.S. degree in Chemistry in 2015 from Paraíba State University, Brazil. During his undergraduate studies he conducted research on polymer-based materials for water remediation. His current work involves the application of stimuli-responsive polymer-based biosensors for label-free detection of pathogens.

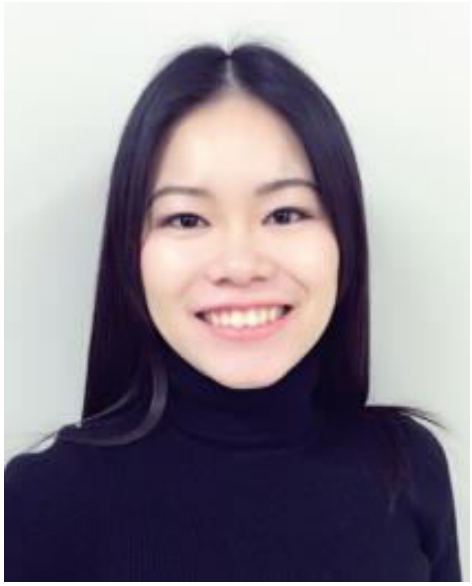

Menglian Wei received her B.S. from Wuhan University in 2011. She joined Prof. Michael J. Serpe's group as a Ph.D. student in 2012 and her research has focused on the development of a novel surface plasmon resonance spectrometer instrument for studying confined polymer brushes, and for improved sensing and biosensing.

Dr. Nduka Ikpo received his B.Sc. Honours in Industrial Chemistry from Abia State University Nigeria and his M.Sc. in Instrumental Analytical Science with emphasis on environmental analysis from Robert Gordon University (RGU) Scotland. He later joined the Kerton Group at Memorial University of Newfoundland (MUN), Canada, where he obtained his M.Sc. (2008) and Ph.D (2013) within the broad areas of Analytical and Synthetic/Green Chemistry. In 2013, Dr. Ikpo moved to the University of Alberta as a postdoctoral researcher in the Department of Renewable Resources, and joined the Serpe Group in the Department of Chemistry in 2016 as Project Coordinator/Lab Manager.

Dr. Yongfeng Gao is currently a postdoctoral researcher in Serpe's group at University of Alberta. Yongfeng received his BSc (2009) and MEng degrees (2012) from Tsinghua University and Beijing University of Chemical Technology, China, respectively. He received his Ph.D. degree on April 2017 under the supervision of Prof. Michael J. Serpe at University of Alberta. His Ph.D. work explored the application of stimuli-responsive microgel-based systems for controlled drug release. His current research is focused on developing color tunable smart materials, bio-inspired structures and sensing devices.

Michael J. Serpe received his B.S. from the University of Central Florida in 2000, his Ph.D. from the Georgia Institute of Technology in 2004 and completed his postdoctoral studies at Duke University in 2009. In the same year he joined the Department of Chemistry at the University of Alberta as an Assistant Professor and was promoted to Associate Professor in 2014. His group's research program is focused on developing new technologies to solve problems associated with health and the environment using fundamental and applied polymer, colloid (nano and microparticles), surface, and materials chemistry.

Acknowledgements

MJS acknowledges funding from the University of Alberta (the Department of Chemistry and the Faculty of Science), the Natural Sciences and Engineering Research Council of Canada (NSERC), the Canada Foundation for Innovation (CFI), the Alberta Advanced Education & Technology Small Equipment Grants Program (AET/SEGP), Grand Challenges Canada, and IC-IMPACTS.

References

1. Lyketsos, C. G.; Colenda, C. C.; Beck, C.; Blank, K.; Doraiswamy, M. P.; Kalunian, D. A.; Yaffe, K., *Am. J. Geriat. Psychiatry* **2006,** *14*, 561-573.
2. Jimbo, K.; Shimizu, T., *Nippon Rinsho* **2012,** *70*, 1338-1342.
3. Amendola, L.; Botrè, F.; Carollo, A. S.; Longo, D.; Zoccolillo, L., *Anal. Chim. Acta* **2002,** *461*, 97-108.
4. Yang, J.; Sun, X.; Feng, Z.; Hao, D.; Wang, M.; Zhao, X.; Sun, C., *Toxicol. Lett.* **2011,** *206*, 306-313.
5. Lin, Z. T.; Gu, J. H.; Li, C. H.; Lee, T. R.; Xie, L. X.; Chen, S.; Cao, P. Y.; Jiang, S.; Yuan, Y. L.; Hong, X.; Wang, H. T.; Wang, D. Z.; Wang, X. F.; Jiang, G. B.; Heon, M.; Wu, T. F., *Adv. Mater.* **2017,** *29*, 1702090.
6. Liu, Z. M.; Rong, Q. F.; Ma, Z. F.; Han, H. L., *Biosens. Bioelectron.* **2015,** *65*, 307-313.
7. Wang, L. Y.; Shan, J.; Feng, F.; Ma, Z. F., *Anal. Chim. Acta* **2016,** *911*, 108-113.
8. Wang, L. Y.; Liu, N.; Ma, Z. F., *J. Mater. Chem. B* **2015,** *3*, 2867-2872.
9. Wang, J.; Wang, Y.; Qiu, H.; Sun, L.; Dai, X.; Pan, J.; Yan, Y., *Sci. Rep.* **2017,** *7,* 46635.
10. Ye, W.; Huang, H.; Yang, W.; Wang, X.; Ren, C.; Hu, Q.; Li, Y.; Ren, B., *Analyst* **2017,** *142*, 3459-3467.
11. Dutta, P.; Chakravarty, S.; Sarma, N. S., *RSC Adv.* **2016,** *6*, 3680-3689.
12. Li, T.; Gao, Z.; Wang, N.; Zhou, Z.; Xu, W.; Zheng, J.; Yang, W., *RSC Adv.* **2016,** *6*, 54615-54622.
13. Faraz, M.; Shakir, M.; Khare, N., *New J. Chem.* **2017,** 41, 5784-5793.
14. Wei, X.; Zhou, Z.; Hao, T.; Li, H.; Yan, Y., *RSC Adv.* **2015,** *5*, 19799-19806.
15. Zhu, X.; Zhang, K.; Wang, C.; Guan, J.; Yuan, X.; Li, B., *Sci. Rep.* **2016,** *6*, 38657.
16. Apodaca, D. C.; Pernites, R. B.; Ponnapati, R.; Del Mundo, F. R.; Advincula, R. C., *Macromolecules* **2011,** *44*, 6669-6682.
17. Chen, X.; Kang, S.; Kim, M. J.; Kim, J.; Kim, Y. S.; Kim, H.; Chi, B.; Kim, S. J.; Lee, J. Y.; Yoon, J., *Angew. Chem.* **2010,** *49*, 1422-1425.
18. Chen, X., *Anal. Methods* **2015,** *7*, 2800-2805.
19. Kuang, K. S. C.; Quek, S. T.; Koh, C. G.; Cantwell, W. J.; Scully, P., *Journal of Sensors* **2009,** 312053.
20. Bandodkar, A. J.; Wang, J., *Trends Biotechnol.* **2014,** *32*, 363-371.
21. Bajaj, A.; Miranda, O. R.; Kim, I.-B.; Phillips, R. L.; Jerry, D. J.; Bunz, U. H.; Rotello, V. M., *Proc. Natl. Acad. Sci. U.S.A* **2009,** *106*, 10912-10916.

22. Yang, G.-Z.; Yang, G., *Springer* **2006**, Vol. 1.
23. Stenken, J. A.; Poschenrieder, A. J., *Anal. Chim. Acta* **2015,** *853*, 95-115.
24. Schley, G.; Koberle, C.; Manuilova, E.; Rutz, S.; Forster, C.; Weyand, M.; Formentini, I.; Kientsch-Engel, R.; Eckardt, K. U.; Willam, C., *PLoS One* **2015,** *10*, 1-23.
25. Liu, L. L.; Liu, F.; Jiang, D. N.; Xiang, G. M.; Liu, C.; Yang, J.; Pu, X. Y., *Sens. Actuators, B* **2016,** *231*, 680-687.
26. Baydemir, G.; Bettazzi, F.; Palchetti, I.; Voccia, D., *Talanta* **2016,** *151*, 141-147.
27. Mazloum-Ardakani, M.; Hosseinzadeh, L.; Khoshroo, A., *J. Electroanal. Chem.* **2015,** *757*, 58-64.
28. Zhou, X. X.; Li, Z. Y.; Zhou, J. F., *Exp. Hematol.* **2017,** *45*, 17-26.
29. Kolomeyevskaya, N.; Eng, K. H.; Khan, A. N. H.; Grzankowski, K. S.; Singel, K. L.; Moysich, K.; Segal, B. H., *Gynecol. Oncol.* **2015,** *138*, 352-357.
30. Zhang, W.; Guo, S. Y.; Stefanio, W.; Carvalho, P.; Jiang, Y. X.; Serpe, M. J., *Anal. Methods* **2016,** *8*, 7847-7867.
31. Sharma, R.; Deacon, S. E.; Nowak, D.; George, S. E.; Szymonik, M. P.; Tang, A. A. S.; Tomlinson, D. C.; Davies, A. G.; McPherson, M. J.; Walti, C., *Biosens. Bioelectron.* **2016,** *80*, 607-613.
32. Aydin, E. B.; Aydin, M.; Sezginturk, M. K., *Biosens. Bioelectron.* **2017,** *97*, 169-176.
33. Sanchez-Tirado, E.; Salvo, C.; Gonzalez-Cortes, A.; Yanez-Sedeno, P.; Langa, F.; Pingarron, J. M., *Anal. Chim. Acta* **2017,** *959*, 66-73.
34. Torres, D. I.; Miranda, M. V.; Campo Dall' Orto, V., *Sens. Actuators, B* **2017,** *239* (Complete), 1016-1025.
35. Cui, M.; Song, Z. L.; Wu, Y. M.; Guo, B.; Fan, X. J.; Luo, X. L., *Biosens. Bioelectron.* **2016,** *79*, 736-741.
36. Luong, J. H. T.; Vashist, S. K., *Biosens. Bioelectron.* **2017,** *89*, 293-304.
37. Abdorahim, M.; Rabiee, M.; Alhosseini, S. N.; Tahriri, M.; Yazdanpanah, S.; Alavi, S. H.; Tayebi, L., *Trends Anal. Chem.* **2016,** *82*, 337-347.
38. Yang, T. T.; Gao, Y. S.; Liu, Z.; Xu, J. K.; Lu, L. M.; Yu, Y. F., *Sens. Actuators, B* **2017,** *239*, 76-84.
39. Hasanzadeh, M.; Shadjou, N.; Lin, Y. H.; de la Guardia, M., *Trends Anal. Chem.* **2017,** *86*, 185-205.
40. Tavakoli, J.; Tang, Y. H., *Polymers* **2017,** *9*, 364.
41. Wang, H. Q.; Han, H. L.; Ma, Z. F., *Bioelectrochemistry* **2017,** *114*, 48-53.
42. Boitard, C.; Rollet, A. L.; Menager, C.; Griffete, N., *Chem. Commun.* **2017,** *53*, 8846-8849.
43. Zaidi, S. A., *Biomater. Sci.* **2017,** *5*, 388-402.
44. Frasco, M. F.; Truta, L. A. A. N. A.; Sales, M. G. F.; Moreira, F. T. C., *Sensors* **2017,** *17*, 523.
45. Luo, J.; Huang, J.; Wu, Y. N.; Sun, J.; Wei, W.; Liu, X. Y., *Biosens. Bioelectron.* **2017,** *94*, 39-46.
46. Ribeiro, J. A.; Pereira, C. M.; Silva, A. F.; Sales, M. G. F., *Anal. Chim. Acta* **2017,** *981*, 41-52.
47. Shen, X. L.; Ma, Y.; Zeng, Q.; Huang, J. Z.; Tao, J.; Wang, L. S., *ChemistrySelect* **2017,** *2*, 6549-6555.
48. Wang, H.; Zhuang, J.; Raghupathi, K. R.; Thayumanavan, S., *Chem. Commun.* **2015,** *51*, 17265-17268.

49. Chen, J. Y.; Liu, Z. J.; Peng, H. P.; Zheng, Y. J.; Lin, Z.; Liu, A. L.; Chen, W.; Lin, X. H., *Biosens. Bioelectron.* **2017,** *98*, 345-349.
50. Campuzano, S.; Yanez-Sedeno, P.; Pingarron, J. M., *Trends Anal. Chem.* **2017,** *86*, 14-24.
51. Krejcovaa, L.; Richtera, L.; Hynek, D.; Labuda, J.; Adama, V., *Biosens. Bioelectron.* **2017,** *97*, 384-399.
52. Diculescu, V. C.; Chiorcea-Paquim, A. M.; Oliveira-Brett, A. M., *Trends Anal. Chem.* **2016,** *79*, 23-36.
53. Hasanzadeh, M.; Shadjou, N.; de la Guardia, M., *Trends Anal. Chem.* **2017,** *91*, 67-76.
54. Mohammadniaei, M.; Lee, T.; Yoon, J.; Lee, D.; Choi, J. W., *Biosens. Bioelectron.* **2017,** *98*, 292-298.
55. Wolfart, F.; Hryniewicz, B. M.; Goes, M. S.; Correa, C. M.; Torresi, R.; Minadeo, M. A. O. S.; de Torresi, S. I. C.; Oliveira, R. D.; Marchesi, L. F.; Vidotti, M., *J. Solid State Electrochem.* **2017,** *21*, 2489-2515.
56. Miodek, A.; Mejri-Omrani, N.; Khoder, R.; Korri-Youssoufi, H., *Talanta* **2016,** *154*, 446-454.
57. Zhu, Q. H.; Gao, F.; Yang, Y. Z.; Zhang, B.; Wang, W.; Hu, Z. S.; Wang, Q. X., *Sens. Actuators, B* **2015,** *207*, 819-826.
58. Tezerjani, M. D.; Benvidi, A.; Rezaeinasab, M.; Jahanbani, S.; Moshtaghioun, S. M.; Youssefi, M.; Zarrini, K., *Anal. Methods* **2016,** *8*, 7507-7515.
59. Gong, Q. J.; Wang, Y. D.; Yang, H. Y., *Biosens. Bioelectron.* **2017,** *89*, 565-569.
60. Labib, M.; Sargent, E. H.; Kelley, S. O., *Chem. Rev.* **2016,** *116*, 9001-9090.
61. Hickey, D. P.; Reid, R. C.; Milton, R. D.; Minteer, S. D., *Biosens. Bioelectron.* **2016,** *77*, 26-31.
62. Pearson-Stuttard, J.; Blundell, S.; Harris, T.; Cook, D. G.; Critchley, J., *Lancet Diabetes Endocrinol.* **2016,** *4*, 148-158.
63. Dekker, L.; Polizzi, K. M., *Curr. Opin. Chem. Biol.* **2017,** *40*, 31-36.
64. Kumar-Krishnan, S.; Chakaravarthy, S.; Hernandez-Rangel, A.; Prokhorov, E.; Luna-Bárcenas, G.; Esparza, R.; Meyyappan, M., *RSC Adv.* **2016,** *6*, 20102-20108.
65. Li, S.; Xiong, J. X.; Chen, C. X.; Chu, F. Q.; Kong, Y.; Deng, L. H., *Materials Technology* **2017,** *32*, 1-6.
66. Yetisen, A. K.; Jiang, N.; Fallahi, A.; Montelongo, Y.; Ruiz- Esparza, G. U.; Tamayol, A.; Zhang, Y. S.; Mahmood, I.; Yang, S. A.; Kim, K. S., *Adv. Mater.* **2017,** *29*, 1606380.
67. Cai, Z.; Luck, L. A.; Punihaole, D.; Madura, J. D.; Asher, S. A., *Chem. Sci.* **2016,** *7*, 4557-4562.
68. Zhang, Q. M.; Berg, D.; Duan, J.; Mugo, S. M.; Serpe, M. J., *ACS Appl. Mater. Interfaces* **2016,** *8*, 27264-27269.
69. Chen, J. Y.; Ji, X. H.; He, Z. K., *Anal. Chem.* **2017,** *89*, 3988-3995.
70. Zeng, H. H.; Qiu, W. B.; Zhang, L.; Liang, R. P.; Qiu, J. D., *Anal. Chem.* **2016,** *88*, 6342-8.
71. Feng, C.; Wang, F.; Dang, Y.; Xu, Z.; Yu, H.; Zhang, W., *Langmuir* **2017,** *33*, 3287-3295.
72. Islam, M. R.; Irvine, J.; Serpe, M. J., *ACS Appl. Mater. Interfaces* **2015,** *7*, 24370-24376.
73. Huang, H.; Serpe, M. J., *J. Appl. Polym. Sci.* **2015,** *132*, 42106.
74. Sorrell, C. D.; Carter, M. C.; Serpe, M. J., *ACS Appl. Mater. Interfaces* **2011,** *3*, 1140-7.
75. Hao, W.; Das, G.; Yoon, H. H., *J. Electroanal. Chem.* **2015,** *747*, 143-148.

76. Das, J.; Sarkar, P., *RSC Adv.* **2016,** *6*, 92520-92533.
77. Li, L.; Long, Y.; Gao, J.-M.; Song, K.; Yang, G., *Nanoscale* **2016,** *8*, 4458-4462.
78. Chaudhari, R.; Joshi, A.; Srivastava, R., *Sci. Rep.* **2017,** *7, 5840*.
79. Chen, Y.; Lu, B.; Chen, Y.; Feng, X., *Sci. Rep.* **2015,** *5,* 11505.
80. Trung, T. Q.; Lee, N. E., *Adv. Mater.* **2016,** *28*, 4338-4372.
81. Choi, S.; Lee, H.; Ghaffari, R.; Hyeon, T.; Kim, D. H., *Adv. Mater.* **2016,** *28*, 4203-4218.
82. Dames, C., *Springer* **2015**, 1782-1790.
83. Becker, J.; Green, C.; Pearson, G., *Transactions of the American Institute of Electrical Engineers* **1946,** *65*, 711-725.
84. Ramakrishna, M.; Karunasiri, G.; Neuzil, P.; Sridhar, U.; Zeng, W., *Sens. Actuators, A* **2000,** *79*, 122-127.
85. Duby, S.; Ramsey, B.; Harrison, D., *Electron. Lett.* **2005,** *41*, 312-314.
86. Martel, R.; Schmidt, T.; Shea, H.; Hertel, T.; Avouris, P., *Appl. Phys. Lett.* **1998,** *73*, 2447-2449.
87. Wawrzynczyk, D.; Bednarkiewicz, A.; Nyk, M.; Strek, W.; Samoc, M., *Nanoscale* **2012,** *4*, 6959-6961.
88. Dong, B.; Cao, B.; He, Y.; Liu, Z.; Li, Z.; Feng, Z., *Adv. Mater.* **2012,** *24*, 1987-1993.
89. Kong, J.; Franklin, N. R.; Zhou, C.; Chapline, M. G.; Peng, S.; Cho, K.; Dai, H., *Science* **2000,** *287*, 622-625.
90. Peng, H.; Stich, M. I.; Yu, J.; Sun, L. n.; Fischer, L. H.; Wolfbeis, O. S., *Adv. Mater.* **2010,** *22*, 716-719.
91. Ryu, S.; Yoo, I.; Song, S.; Yoon, B.; Kim, J.-M., *J. Am. Chem. Soc.* **2009,** *131*, 3800-3801.
92. Liu, H.; Liu, H.; Peng, G.; Chu, P., *Opt. Commun.* **2003,** *219*, 139-142.
93. Jeon, J.; Lee, H. B. R.; Bao, Z., *Adv. Mater.* **2013,** *25*, 850-855.
94. Zeng, W.; Shu, L.; Li, Q.; Chen, S.; Wang, F.; Tao, X. M., *Adv. Mater.* **2014,** *26*, 5310-5336.
95. Takei, K.; Honda, W.; Harada, S.; Arie, T.; Akita, S., *Adv. Healthc. Mater.* **2015,** *4*, 487-500.
96. Xu, L.; Gutbrod, S. R.; Bonifas, A. P.; Su, Y.; Sulkin, M. S.; Lu, N.; Chung, H.-J.; Jang, K.-I.; Liu, Z.; Ying, M., *Nat. Commun.* **2014,** *5*, 3329.
97. Webb, R. C.; Bonifas, A. P.; Behnaz, A.; Zhang, Y.; Yu, K. J.; Cheng, H.; Shi, M.; Bian, Z.; Liu, Z.; Kim, Y.-S., *Nat. Mater.* **2013,** *12*, 938.
98. Kim, D.-H.; Lu, N.; Ma, R.; Kim, Y.-S.; Kim, R.-H.; Wang, S.; Wu, J.; Won, S. M.; Tao, H.; Islam, A., *Science* **2011,** *333*, 838-843.
99. Khodagholy, D.; Doublet, T.; Quilichini, P.; Gurfinkel, M.; Leleux, P.; Ghestem, A.; Ismailova, E.; Hervé, T.; Sanaur, S.; Bernard, C., *Nat. Commun.* **2013,** *4*, 1575.
100. Kaltenbrunner, M.; Sekitani, T.; Reeder, J.; Yokota, T.; Kuribara, K.; Tokuhara, T.; Drack, M.; Schwödiauer, R.; Graz, I.; Bauer-Gogonea, S., *Nature* **2013,** *499*, 458-463.
101. Yokota, T.; Inoue, Y.; Terakawa, Y.; Reeder, J.; Kaltenbrunner, M.; Ware, T.; Yang, K.; Mabuchi, K.; Murakawa, T.; Sekino, M., *Proc. Natl. Acad. Sci. U.S.A* **2015,** *112*, 14533-14538.
102. Jia, W.; Bandodkar, A. J.; Valdés-Ramírez, G.; Windmiller, J. R.; Yang, Z.; Ramírez, J.; Chan, G.; Wang, J., *Anal. Chem.* **2013,** *85*, 6553-6560.
103. Bandodkar, A. J.; Molinnus, D.; Mirza, O.; Guinovart, T.; Windmiller, J. R.; Valdés-Ramírez, G.; Andrade, F. J.; Schöning, M. J.; Wang, J., *Biosens. Bioelectron.* **2014,** *54*, 603-609.

104. Rose, D. P.; Ratterman, M. E.; Griffin, D. K.; Hou, L.; Kelley-Loughnane, N.; Naik, R. R.; Hagen, J. A.; Papautsky, I.; Heikenfeld, J. C., *IEEE Trans. Biomed. Eng.* **2015,** *62*, 1457-1465.
105. Al-Omari, M.; Sel, K.; Mueller, A.; Edwards, J.; Kaya, T., *J. Appl. Phys.* **2014,** *115*, 203107.
106. Mena-Bravo, A.; De Castro, M. L., *J. Pharm. Biomed. Anal.* **2014,** *90*, 139-147.
107. Sonner, Z.; Wilder, E.; Heikenfeld, J.; Kasting, G.; Beyette, F.; Swaile, D.; Sherman, F.; Joyce, J.; Hagen, J.; Kelley-Loughnane, N., *Biomicrofluidics* **2015,** *9*, 031301-031319.
108. Desax, M.-C.; Ammann, R. A.; Hammer, J.; Schoeni, M. H.; Barben, J.; Group, S. P. R. R., *Eur. J. Pediatr.* **2008,** *167*, 299-304.
109. Selvam, A. P.; Muthukumar, S.; Kamakoti, V.; Prasad, S., *Sci. Rep.* **2016,** *6*, 23111.
110. Glaros, C.; Fotiadis, D.; Likas, A.; Stafylopatis, A. In *A wearable intelligent system for monitoring health condition and rehabilitation of running athletes*, Information Technology Applications in Biomedicine, 2003. 4th International IEEE EMBS Special Topic Conference on, IEEE: 2003; 276-279.
111. Corrie, S.; Coffey, J.; Islam, J.; Markey, K.; Kendall, M., *Analyst* **2015,** *140*, 4350-4364.
112. Gao, W.; Emaminejad, S.; Nyein, H. Y. Y.; Challa, S.; Chen, K.; Peck, A.; Fahad, H. M.; Ota, H.; Shiraki, H.; Kiriya, D., *Nature* **2016,** *529*, 509-514.
113. Cerqueira, G. C.; Earl, A. M.; Ernst, C. M.; Grad, Y. H.; Dekker, J. P.; Feldgarden, M.; Chapman, S. B.; Reis-Cunha, J. L.; Shea, T. P.; Young, S.; Zeng, Q.; Delaney, M. L.; Kim, D.; Peterson, E. M.; O'Brien, T. F.; Ferraro, M. J.; Hooper, D. C.; Huang, S. S.; Kirby, J. E.; Onderdonk, A. B.; Birren, B. W.; Hung, D. T.; Cosimi, L. A.; Wortman, J. R.; Murphy, C. I.; Hanage, W. P., *Proc. Natl. Acad. Sci. U.S.A* **2017,** *114*, 1135-1140.
114. Rex, J. H.; Talbot, G. H.; Goldberger, M. J.; Eisenstein, B. I.; Echols, R. M.; Tomayko, J. F.; Dudley, M. N.; Dane, A., *Clin. Infect. Dis.* **2017,** *65*, 141-146.
115. Lazcka, O.; Del Campo, F. J.; Munoz, F. X., *Biosens. Bioelectron.* **2007,** *22*, 1205-1217.
116. Fournier, P. E.; Drancourt, M.; Colson, P.; Rolain, J. M.; La Scola, B.; Raoult, D., *Nat. Rev. Microbiol.* **2013,** *11*, 574-585.
117. Organization, W. H., *Guidelines for Drinking-Water Quality*. World Health Organization: 2004; Vol. 1.
118. Kelley, S. O., *ACS Sens.* **2017,** *2*, 193-197.
119. Kamoun, E. A.; Kenawy, E. R. S.; Chen, X., *J. Adv. Res.* **2017,** *8*, 217-233.
120. Jeong, K. H.; Park, D.; Lee, Y. C., *J. Polym. Res.* **2017,** *24,* 112.
121. Xinming, L.; Yingde, C.; Lloyd, A. W.; Mikhalovsky, S. V.; Sandeman, S. R.; Howel, C. A.; Liewen, L., *Cont. Lens Anterior Eye* **2008,** *31*, 57-64.
122. Sadat Ebrahimi, M. M.; Voss, Y.; Schonherr, H., *ACS Appl. Mater. Interfaces* **2015,** *7*, 20190-9.
123. Sheikhzadeh, E.; Chamsaz, M.; Turner, A. P. F.; Jager, E. W. H.; Beni, V., *Biosens. Bioelectron.* **2016,** *80*, 194-200.
124. Giovanni, M.; Setyawati, M. I.; Tay, C. Y.; Qian, H.; Kuan, W. S.; Leong, D. T., *Adv. Funct. Mater.* **2015,** *25*, 3840-3846.
125. Bai, H.; Chen, H.; Hu, R.; Li, M.; Lv, F.; Liu, L.; Wang, S., *ACS Appl. Mater. Interfaces* **2016,** *8*, 31550-31557.
126. Mazrad, Z. A. I.; In, I.; Lee, K. D.; Park, S. Y., *Biosens. Bioelectron.* **2017,** *89*, 1026-1033.
127. Erturk, G.; Mattiasson, B., *Sensors* **2017,** *17,* 288.

128. van Grinsven, B.; Eersels, K.; Akkermans, O.; Ellermann, S.; Kordek, A.; Peeters, M.; Deschaume, O.; Bartic, C.; Diliën, H.; Steen Redeker, E., *ACS Sens.* **2016,** *1*, 1140-1147.
129. van Grinsven, B.; Eersels, K.; Peeters, M.; Losada-Perez, P.; Vandenryt, T.; Cleij, T. J.; Wagner, P., *ACS Appl. Mater. Interfaces* **2014,** *6*, 13309-13318.
130. Redeker, E. S.; Eersels, K.; Akkermans, O.; Royakkers, J.; Dyson, S.; Nurekeyeva, K.; Ferrando, B.; Cornelis, P.; Peeters, M.; Wagner, P.; Dilien, H.; van Grinsven, B.; Cleij, T. J., *ACS Infect. Dis.* **2017,** *3*, 388-397.
131. Chen, S. F.; Chen, X. Q.; Zhang, L. J.; Gao, J. J.; Ma, Q., *ACS Appl. Mater. Interfaces* **2017,** *9*, 5430-5436.
132. Stuart, M. A. C.; Huck, W. T.; Genzer, J.; Müller, M.; Ober, C.; Stamm, M.; Sukhorukov, G. B.; Szleifer, I.; Tsukruk, V. V.; Urban, M., *Nat. Mater.* **2010,** *9*, 101-113.
133. Teratanatorn, P.; Hoskins, R.; Swift, T.; Douglas, C. W. I.; Shepherd, J.; Rimmer, S., *Biomacromolecules* **2017,** *18*, 2887-2899.
134. Shepherd, J.; Sarker, P.; Swindells, K.; Douglas, I.; MacNeil, S.; Swanson, L.; Rimmer, S., *J. Am. Chem. Soc.* **2010,** *132*, 1736-1737.
135. Tchounwou, P. B.; Yedjou, C. G.; Patlolla, A. K.; Sutton, D. J., *Springer* **2012,** Vol. 1.
136. He, Z. L.; Yang, X. E.; Stoffella, P. J., *J. Trace Elem. Med. Biol.* **2005,** *19*, 125-140.
137. Hu, Y.; Liu, Z.; Zhan, H.; Hu, L.; Cui, L.; Wang, K., *Anal. Methods* **2017,** 9, 3870-3875.
138. Xu, F.; Cui, Z.-M.; Li, H.; Luo, Y.-L., *RSC Adv.* **2017,** *7*, 7431-7441.
139. Arslan, O.; Uyar, T., *Nanoscale* **2017,** *9*, 9606-9614.
140. Arslan, O.; Aytac, Z.; Uyar, T., *J. Mater. Chem. C* **2017,** *5*, 1816-1825.
141. Yu, J.; Wang, X.; Kang, Q.; Li, J.; Shen, D.; Chen, L., *Environ. Sci. Nano* **2017,** *4*, 493-502.
142. Li, G.; Tao, F.; Liu, Q.; Wang, L.; Wei, Z.; Zhu, F.; Chen, W.; Sun, H.; Zhou, Y., *New J. Chem.* **2016,** *40*, 4513-4518.
143. Wang, T.; Guo, Y.; Wan, P.; Sun, X.; Zhang, H.; Yu, Z.; Chen, X., *Nanoscale* **2017,** *9*, 869-874.
144. Balamurugan, A.; Lee, H.-i., *Macromolecules* **2015,** *48*, 1048-1054.
145. Bai, X.; Li, Y.; Ye, Z., *New J. Chem.* **2016,** *40*, 8815-8822.
146. Gao, Z.; Liu, G. G.; Ye, H.; Rauschendorfer, R.; Tang, D.; Xia, X., *Anal. Chem.* **2017,** *89*, 3622-3629.
147. Lin, Z. H.; Zhu, G.; Zhou, Y. S.; Yang, Y.; Bai, P.; Chen, J.; Wang, Z. L., *Angew. Chem.* **2013,** *52*, 5065-5069.
148. Zahir, F.; Rizwi, S. J.; Haq, S. K.; Khan, R. H., *Environ. Toxicol. Pharmacol.* **2005,** *20*, 351-360.
149. Vallejos, S.; Reglero, J. A.; García, F. C.; García, J. M., *J. Mater. Chem. A* **2017,** *5*, 13710-13716.
150. Harris, E. D., *J. Trace Elem. Exp.Med.* **2001,** *14*, 207-210.
151. Koval, I. A.; Gamez, P.; Belle, C.; Selmeczi, K.; Reedijk, J., *Chem. Soc. Rev.* **2006,** *35*, 814-840.
152. Gupta, V. K.; Singh, L.; Singh, R.; Upadhyay, N.; Kaur, S.; Sethi, B., *J. Mol. Liq.* **2012,** *174*, 11-16.
153. Yang, Y.-K.; Yook, K.-J.; Tae, J., *J. Am. Chem. Soc.* **2005,** *127*, 16760-16761.
154. Hassanzadeh, J.; Khataee, A.; Oskoei, Y. M.; Fattahi, H.; Bagheri, N., *New J. Chem.* **2017,** *41*, 10659-10667.

155. Shriver-Lake, L. C.; Breslin, K. A.; Charles, P. T.; Conrad, D. W.; Golden, J. P.; Ligler, F. S., *Anal. Chem.* **1995,** *67*, 2431-2435.
156. Xu, D.; Zhu, W.; Wang, C.; Tian, T.; Li, J.; Lan, Y.; Zhang, G.; Zhang, D.; Li, G., *Chem. Commun.* **2014,** *50*, 14133-14136.